^{231}Pa and ^{230}Th in the ocean model of the Community Earth System Model (CESM1.3)

Sifan Gu[1], Zhengyu Liu[1,2]

[1]Department of Atmospheric and Oceanic Sciences and Center for Climate Research, University of Wisconsin-Madison, Madison, WI, USA

2. Now, affiliated with: Atmospheric Science Program, Department of Geography, Ohio State University

Correspondence to: Sifan Gu (sgu28@wisc.edu)

Abstract

Sediment ^{231}Pa/^{230}Th activity ratio is emerging as an important proxy for deep ocean circulation in the past. In order to allow for a direct model-data comparison and to improve our understanding of sediment ^{231}Pa/^{230}Th activity ratio, we implement ^{231}Pa and ^{230}Th in the ocean component of the Community Earth System Model (CESM). In addition to the p-coupled ^{231}Pa and ^{230}Th that is fully coupled with the active marine ecosystem module, another form of p-fixed ^{231}Pa and ^{230}Th have also been implemented with prescribed particle flux fields of the present climate. The comparison of the two forms of ^{231}Pa and ^{230}Th helps to isolate the influence of the particle fluxes from that of circulation. Under present day climate forcing, our model is able to simulate water column ^{231}Pa and ^{230}Th activity and sediment ^{231}Pa/^{230}Th activity ratio in good agreement with available observations. In addition, the p-coupled and p-fixed sediment ^{231}Pa/^{230}Th activity ratios behave similarly over large areas of low productivity on long timescale to freshwater forcing, but can differ substantially in some regions of high productivity and on short timescale, indicating the importance of biological productivity in addition to physical circulation. Therefore, our model provides a potentially powerful tool to help our interpretation of sediment ^{231}Pa/^{230}Th reconstructions and to improve our understanding of past ocean circulation and climate changes.

1. Introduction

Sediment $^{231}Pa/^{230}Th$ activity ratio has been used as a proxy to reconstruct ocean circulation in the past (e.g. Yu et al. 1996; McManus et al. 2004; Gherardi et al. 2009). ^{231}Pa (32.5 ka half-life) and ^{230}Th (75.2 ka half-life) are produced at a constant rate approximately uniformly in the ocean by the α decay of ^{235}U and ^{234}U, respectively, with a production activity ratio of 0.093 (Henderson and Anderson, 2003). Water column ^{231}Pa and ^{230}Th are subject to particle scavenging and transport to sediments (Bacon and Anderson, 1982; Nozaki et al., 1987). Differential scavenging efficiency results in different ocean residence time: ^{231}Pa has a residence time of approximately 111 years and ^{230}Th has a residence time of approximately 26 years (Yu et al., 1996). Longer residence time of ^{231}Pa than ^{230}Th makes ^{231}Pa more subject to ocean transport and therefore in modern ocean about 45% of ^{231}Pa produced in the Atlantic is transported to the Southern Ocean (Yu et al., 1996), resulting a lower than 0.093 sediment $^{231}Pa/^{230}Th$ activity ratio in the North Atlantic and higher than 0.093 sediment $^{231}Pa/^{230}Th$ activity ratio in the Southern Ocean.

The application of the principle above to interpret sediment $^{231}Pa/^{230}Th$ as the strength of Atlantic Meridional Overturning Circulation (AMOC), however, can be complicated by other factors, leading to uncertainties in using $^{231}Pa/^{230}Th$ as a proxy for paleocirculation (Keigwin and Boyle, 2008; Lippold et al., 2009; Scholten et al., 2008). In addition to ocean transport, sediment $^{231}Pa/^{230}Th$ is also influenced by particle flux and composition (Chase et al., 2002; Geibert and Usbeck, 2004; Scholten et al., 2008; Siddall et al., 2007; Walter et al., 1997). The region of a higher particle flux tends to have a higher $^{231}Pa/^{230}Th$ (Kumar et al., 1993; Yong Lao et al., 1992), which is referred to as the "particle flux effect" (Siddall et al., 2005). High particle flux in the water column in a region will favor the removal of isotopes into the sediment, which leads to more isotopes transported into this region due to the down-gradient diffusive flux into this region and subsequently more removal of isotopes into the sediment. Since ^{231}Pa has a longer residence time, this effect is

more prominent on ^{231}Pa than on ^{230}Th and therefore sediment $^{231}Pa/^{230}Th$ will be higher in high productivity regions. Also, opal is able to scavenge ^{231}Pa much more effectively than ^{230}Th, leading to higher $^{231}Pa/^{230}Th$ in high opal flux regions such as the Southern Ocean (Chase et al., 2002). Moreover, sediment $^{231}Pa/^{230}Th$ is suggested to record circulation change only within 1000 m above the sediment, instead of the whole water column, complicating the interpretation of sediment $^{231}Pa/^{230}Th$ reconstructions (Thomas et al., 2006). For example, sediment $^{231}Pa/^{230}Th$ approaching 0.093 during Heinrich Stadial event 1(HS1) from the subtropical North Atlantic is interpreted as the collapse of the Atlantic Meridional Overturning Circulation (AMOC) (McManus et al., 2004). If sediment $^{231}Pa/^{230}Th$ only records deepest water mass, it is possible that during HS1, AMOC shoals, as opposed to fully collapse, yet an increase of deep water imported from the Southern Ocean featuring high $^{231}Pa/^{230Th}$ can increase the sediment $^{231}Pa/^{230}Th$ approaching the production ratio (0.093) (Thomas et al., 2006). All these suggest the importance of incorporating ^{231}Pa and ^{230}Th into climate models for a direct model-data comparison for a thorough understanding of sediment $^{231}Pa/^{230}Th$ as well as past ocean circulation.

^{231}Pa and ^{230}Th have been simulated in previous modeling studies (Dutay et al., 2009; Luo et al., 2010; Marchal et al., 2000; Rempfer et al., 2017; Siddall et al., 2005). Marchal et al., (2000) simulates ^{231}Pa and ^{230}Th in a zonally averaged circulation model, using the reversible scavenging model of Bacon and Anderson, (1982). One step further, Siddall et al. (2005) extends Marchal et al., (2000) by including particle dissolution with prescribed particle export production in a 3-D circulation model. Rempfer et al., (2017) further couples ^{231}Pa and ^{230}Th with active biogeochemical model and includes boundary scavenging and sediment resuspensions to improve model performance in simulating water column ^{231}Pa and ^{230}Th concentration. Here we follow previous studies to implement ^{231}Pa and ^{230}Th into the Community Earth System Model (CESM). Our model ^{231}Pa and ^{230}Th are coupled with active marine ecosystem model ("p-coupled") and therefore can be used to study the impact of ecosystem change on ^{231}Pa and ^{230}Th directly. To help to understand the influence of the particle flux, we have also implemented a "p-fixed"

version of ^{231}Pa and ^{230}Th, for which the particle fluxes are fixed at prescribed values. By comparing the p-fixed ^{231}Pa and ^{230}Th with the p-coupled ^{231}Pa and ^{230}Th, we will be able to separate the effect of circulation change from particle field change. In addition, the p-fixed ^{231}Pa and ^{230}Th can be run without the marine ecosystem module, reducing computational cost by a factor of 3 in the ocean-alone model simulation and therefore making it a computationally efficient tracer for sensitivity studies.

This paper describes the details of ^{231}Pa and ^{230}Th in CESM and serves as a reference for future studies using this tracer module. In section 2, we describe the model and the implementation of ^{231}Pa and ^{230}Th. In sections 3, we describe the experimental design. We will finally compare simulated ^{231}Pa and ^{230}Th fields with observations, show model sensitivities on the parameter and also sediment ^{231}Pa/^{230}Th ratio response to freshwater forcing in Section 4.

2. Model Description

2.1 Physical Ocean Model

We implement ^{231}Pa and ^{230}Th in the ocean model (Parallel Ocean Program version 2, POP2) (Danabasoglu et al., 2012) of CESM (Hurrell et al., 2013). CESM is a state-of-the-art coupled climate model and studies describing model components and analyzing results can be found in a special collection in Journal of Climate (http://journals.ametsoc.org/topic/ccsm4-cesm1). We run the ocean-alone model, which is coupled to data atmosphere, land, ice and river runoff under the normal year forcing of CORE-II data (Large and Yeager, 2008), using the low-resolution version of POP2 with a nominal 3° horizontal resolution and 60 vertical layers.

2.2 Biogeochemical component (BGC)

CESM has incorporated a marine ecosystem module that simulates biological variables (Moore et al., 2013). The marine ecosystem module has been validated against present day observations extensively (e.g. Doney et al., 2009; Long et al., 2013; Moore et al., 2002, 2004; Moore and Braucher, 2008). The implementation of ^{231}Pa and ^{230}Th requires particle fields: $CaCO_3$, opal and particulate organic carbon

(POC). These particle fields can be obtained from the ecosystem driver from the ecosystem module (Jahn et al., 2015). The ecosystem module simulates the particle fluxes in reasonable agreement with the present day observations. The pattern and magnitude of the annual mean particle fluxes ($CaCO_3$, opal, POC) leaving the euphotic zone at 105m are similar to the satellite observations (Fig. 7.2.5 and 9.2.2 in Sarmiento and Gruber 2006) (Fig. 1 a∼c): particle fluxes are higher in the high productivity regions such as high latitudes and equatorial Pacific; opal flux is high in the Southern Ocean. The remineralization scheme of particle is based on the ballast model of Armstrong et al., (2002). Detailed parameterizations for particle remineralization are documented in Moore et al., (2004) with temperature dependent remineralization length scales for POC and opal. We do not consider dust because it is suggested to be unimportant for ^{231}Pa and ^{230}Th fractionation (Chase et al., 2002; Siddall et al., 2005).

2.3 ^{231}Pa and ^{230}Th implementation

^{231}Pa and ^{230}Th are produced from the α decay of ^{235}U and ^{234}U uniformly everywhere at constant rate β^i (β^{Pa} = 2.33*10^{-3} dpm m^{-3} yr^{-1}, β^{Th} = 2.52*10^{-2} dpm m^{-3} yr^{-1}). ^{231}Pa and ^{230}Th are also subjective to radioactive decay with the decay constant of λ^i (λ^{Pa} = 2.13*10^{-5} yr^{-1}, λ^{Th} = 9.22*10^{-6} yr^{-1}).

Another important process contributes to ^{231}Pa and ^{230}Th activity is the reversible scavenging by sinking particles (Bacon and Anderson, 1982), which describes the adsorption of isotopes onto sinking particles and desorption after the dissolution of particles. This process transports ^{231}Pa and ^{230}Th downward and leads to a general increase of ^{231}Pa and ^{230}Th activity with depth. The reversible scavenging considers total isotope activity (A_t^i) as two categories (Eq. (1)): dissolved isotopes (A_d^i) and particulate isotopes (A_p^i) (superscript i refers to ^{231}Pa and ^{230}Th) and A_p^i is the sum of the isotopes associated with different particle types ($A_{j,p}^i$) (subscript j refers to different particle types: $CaCO_3$, opal and POC):

$$A_t^i = A_d^i + A_p^i = A_d^i + \sum_j A_{j,p}^i \quad (1)$$

Dissolved and particulate isotopes are assumed to be in equilibrium, which is a reasonable assumption in the open ocean (Bacon and Anderson, 1982; Henderson et al., 1999; Moore and Hunter, 1985). The ratio between the particulate isotope activity and the dissolved isotope activity is set by a partition coefficient, K (Eq. (2)):

$$K_j^i = \frac{A_{j,p}^i}{A_d^i \cdot R_j} \quad (2)$$

, where R_j is the ratio of particle concentration (C_j) to the density of seawater (1024.5 kg m^{-3}). Subscript j refers to different particle types ($CaCO_3$, opal and POC). Values of partition coefficient K used in our control simulation follows Chase et al., 2002 and Siddall et al., 2005 (Table 2).

Particulate isotopes (A_p^i) will be transported by sinking particles, which is described by $w_S \frac{\partial A_p^i}{\partial z}$, where w_s is sinking velocity. We don't differentiate between slow sinking small particles and rapid sinking large particles as in Dutay et al., (2009) and consider all particles as slowly sinking small particles with sinking velocity of w_s =1000 m yr^{-1} (Arsouze et al., 2009; Dutay et al., 2009; Kriest, 2002) as in Rempfer et al., (2017) and Siddall et al., (2005). Any particulate isotopes (A_p^i) at the ocean bottom layer are removed from the ocean as sediment, which is the sink for the isotope budget. Detailed vertical differentiation scheme to calculate this term in the model is in the supplementary material. The reversible scavenging scheme applied here is the same as the neodymium implementation in POP2 (Gu et al., 2017).

Particle fields used in the reversible scavenging can be either prescribed or simultaneously generated from the marine ecosystem module. Therefore, two forms of ^{231}Pa and ^{230}Th are implemented in POP2: "p-fixed" and "p-coupled". P-fixed ^{231}Pa and ^{230}Th use particle fluxes prescribed as annual mean particle fluxes generated from the marine ecosystem module under present day climate forcing (Fig.1). P-coupled ^{231}Pa and ^{230}Th use particle fluxes computed simultaneously from the

marine ecosystem module. P-fixed and p-coupled ^{231}Pa and ^{230}Th can be turned on at the case build time and the p-coupled ^{231}Pa and ^{230}Th requires the ecosystem module to be turned on at the same time.

Therefore, the conservation equation for ^{231}Pa and ^{230}Th activity can be written as

$$\frac{\partial A_t^i}{\partial t} = \beta^i - \lambda^i A_t^i - w_s \frac{\partial A_p^i}{\partial z} + Transport \quad (3),$$

where the total isotope activity is controlled by decay from U (first term), radioactive decay (second term), reversible scavenging (third term) and physical transport by the ocean model (fourth term, including advection, convection and diffusion). A_p^i can be calculated by combining Eq. (1) and Eq. (2):

$$A_t^i = A_d^i + A_d^i \cdot (K_{POC}^i \cdot R_{POC} + K_{CaCO_3}^i \cdot R_{CaCO_3} + K_{opal}^i \cdot R_{opal})$$
$$= A_d^i \cdot (1 + K_{POC}^i \cdot R_{POC} + K_{CaCO_3}^i \cdot R_{CaCO_3} + K_{opal}^i \cdot R_{opal}), \quad (4)$$

which leads to

$$A_d^i = \frac{A_t^i}{1 + K_{POC}^i \cdot R_{POC} + K_{CaCO_3}^i \cdot R_{CaCO_3} + K_{opal}^i \cdot R_{opal}}, \quad (5)$$

put this back to Eq.(1), we get

$$A_p^i = A_t^i \cdot (1 - \frac{1}{1 + K_{POC}^i \cdot R_{POC} + K_{CaCO_3}^i \cdot R_{CaCO_3} + K_{opal}^i \cdot R_{opal}}) \quad (6)$$

Comparing with previous studies of modeling ^{231}Pa and ^{230}Th, our p-fixed version is the same as Siddall et al., (2002), except that different prescribed particle fluxes are used. The p-coupled version allows coupling to biogeochemical module, which is similar in Rempfer et al., (2017), but we do not include boundary scavenging and sediment resuspensions as in Rempfer et al., (2017) because boundary scavenging and sediment resuspensions are suggested to be unimportant to influence the relationship between $^{231}Pa_p/^{230}Th_p$ and AMOC strength (Rempfer et al., 2017).

3. Experiments

We run a control experiment (CTRL) and two experiments with different partition coefficients to show model sensitivity to partition coefficient. We have both p-fixed and p-coupled ^{231}Pa and ^{230}Th in CTRL, but only p-fixed ^{231}Pa and ^{230}Th in sensitivity experiments. Equilibrium partition coefficients for ^{231}Pa and ^{230}Th vary among different particle types and the magnitude of the partition coefficients for different particle types remains uncertain (Chase et al., 2002; Chase and Robert F, 2004; Luo and Ku, 1999). Since the control experiment in Siddall et al., (2005) is able to simulate major features of ^{231}Pa and ^{230}Th distributions, we use the partition coefficients from the control experiment in Siddall et al., (2005) in our CTRL (Table 2). Two sensitivity experiments are performed with decreased (EXP_1) and increased (EXP_2) partition coefficients by a factor of 5 (Table 2).

All the experiments are ocean-alone experiments with the normal year forcing by CORE-II data (Large and Yeager, 2008). The ^{231}Pa and ^{230}Th activities are initiated from 0 in CTRL and are integrated for 2,000 model years until equilibrium is reached. EXP_1 and EXP_2 are initiated from 1,400 model year in CTRL and are integrated for another 800 model years to reach equilibrium.

Since sediment ^{231}Pa/^{230}Th in North Atlantic has been used to reflect the strength of AMOC, to test how sediment ^{231}Pa/^{230}Th in our model responds to the change of AMOC, we carried out a fresh water perturbation experiment (HOSING) with both p-fixed and p-coupled ^{231}Pa and ^{230}Th. Starting from 2,000 model year of CTRL, a freshwater flux of 1 Sv is imposed over the North Atlantic region of 50°N~70°N and the experiment is integrated for 1400 model years until both p-fixed and p-coupled sediment ^{231}Pa/^{230}Th ratio have reached quasi-equilibrium. The partition coefficients used in HOSING are the same as in CTRL.

4. Results

4.1 Control Experiment

P-fixed and p-coupled version of ^{231}Pa and ^{230}Th in CTRL show identical results (Fig. 2-4). P-fixed and p-coupled dissolved and particulate ^{231}Pa and ^{230}Th in CTRL are highly correlated with each other with correlations larger than 0.995 and

regression coefficients are all near 1.0 (R^2>0.995). The correlation coefficient between p-fixed and p-coupled sediment $^{231}Pa/^{230}Th$ activity ratios in CTRL is 0.99 and the regression coefficient is 0.9 (R^2=0.98) (Fig. 4a). This is expected because the particle fields used in p-fixed version are the climatology of the particle fields used in the p-coupled version. Therefore, under the same climate forcing, p-fixed and p-coupled version of ^{231}Pa and ^{230}Th should be very similar. For the discussion of results in CTRL below, we only discuss the p-fixed ^{231}Pa and ^{230}Th.

The residence time of both ^{231}Pa and ^{230}Th in CTRL are comparable with observations. The residence time is calculated as the ratio of global average total isotope activity and the radioactive ingrowth of the isotope. Residence time in CTRL is 118 yr for ^{231}Pa and 33 yr for ^{230}Th (Table 2), which are of the same magnitude as 111 yr for ^{231}Pa and 26 yr for ^{230}Th in observation (Yu et al., 1996).

CTRL can simulate the general features of dissolved water column ^{231}Pa and ^{230}Th activities. Dissolved ^{231}Pa and ^{230}Th activities increase with depth in CTRL, as shown in two GEOTRACES transects (Deng et al., 2014; Hayes et al., 2015) in the Atlantic (Fig. 2 and 3). The dissolved ^{231}Pa and ^{230}Th activities in CTRL are also at the same order of magnitude as in observations in the most of the ocean, except that simulated values are larger than observations in abyssal, which is also the case in Siddall et al., (2005) and Rempfer et al., (2017) (their Fig. 2 and 3, experiment Re3d). Our model is unable to simulate the realistic dissolved ^{231}Pa and ^{230}Th activities in abyssal because boundary scavenging and sediment resuspensions are not included in our model. With boundary scavenging and sediment resuspensions added, dissolved ^{231}Pa and ^{230}Th activities in the abyssal should be reduced (Rempfer et al., 2017).

A more quantitative model-data comparison is shown in Fig. 5. The linear regression coefficient, an indication of model ability to simulate ^{231}Pa and ^{230}Th activity (Dutay et al., 2009), is near 1.0 for dissolved ^{231}Pa and ^{230}Th (1.02 for $[^{231}Pa]_d$ and 1.14 for $[^{230}Th]_d$), suggesting that CTRL can simulate the dissolved ^{231}Pa and ^{230}Th in good agreement with observations. However, the simulation of the particulate activity is not as good as the dissolved activity. Particulate activity is overall larger than observations in the surface ocean and smaller than observation

in the deep ocean for both particulate ^{231}Pa and ^{230}Th. The regression coefficient for particulate ^{231}Pa and ^{230}Th is 0.02 for $[^{231}Pa]_p$ and 0.05 for $[^{230}Th]_p$. The poor performance in simulating water column particulate ^{231}Pa and ^{230}Th activities is also in previous modeling studies (Dutay et al., 2009; Siddall et al., 2005), because of similar modelling scheme are applied. However, the simulated $^{231}Pa_p/^{230}Th_p$ is reasonable. The $^{231}Pa_p/^{230}Th_p$ along two GEOTRACES tracks (Fig. 2 and 3) show the similar pattern and magnitude as in Rempfer et al., (2017). Decrease of $^{231}Pa_p/^{230}Th_p$ with depth is well simulated, which is suggested to be caused by the lateral transport of ^{231}Pa from North Atlantic to Southern Ocean by AMOC (Gherardi et al., 2009; Lippold et al., 2011, 2012a; Luo et al., 2010; Rempfer et al., 2017).

The sediment ^{231}Pa/^{230}Th in CTRL is overall consistent with observations (references of observations are listed in Table 3). The North Atlantic shows low sediment ^{231}Pa/^{230}Th activity ratio as in observations because ^{231}Pa is more subject to transport southward to the Southern Ocean by active ocean circulation than ^{230}Th because of longer residence time. The Southern Ocean maximum in the sediment ^{231}Pa/^{230}Th activity ratio is also simulated in CTRL. High opal fluxes in the Southern Ocean, which preferentially removes ^{231}Pa into sediment ($K_{opal}^{^{231}Pa} > K_{opal}^{^{230}Th}$) (Chase et al., 2002), leading to increased sediment ^{231}Pa/^{230}Th activity ratio. In addition, upwelling in the Southern Ocean brings up deep water enriched with ^{231}Pa, which is transported from the North Atlantic, to shallower depth and further contribute to the scavenging. CTRL can also produce higher sediment ^{231}Pa/^{230}Th activity ratio in regions with high particle production (e.g. the Eastern equatorial Pacific, the North Pacific and the Indian Ocean) due to the "particle flux effect". Specifically, in North Atlantic, the distribution of sediment ^{231}Pa/^{230}Th matches the distribution of particle, especially opal, production: sediment ^{231}Pa/^{230}Th is higher where opal production is high, and vice versa.

4.2 Sensitivity on partition coefficient K

In this section, we show model sensitivity on partition coefficient by increasing and decreasing the partition coefficient, K, by a factor of 5, but keep the

301 relative ratio for different particles the same (Table 2). Our model shows similar
302 model sensitivity as in Siddall et al., (2005) as discussed below.
303 Increasing K will decrease water column dissolved ^{231}Pa and ^{230}Th activities
304 but won't change particulate ^{231}Pa and ^{230}Th too much (Fig. 6). Larger K will lead to
305 more ^{231}Pa and ^{230}Th attached to particles and further buried into sediment, which
306 increases the sink for the ^{231}Pa and ^{230}Th budget. With the sources for ^{231}Pa and
307 ^{230}Th staying the same, dissolved ^{231}Pa and ^{230}Th will be reduced. Increasing K will
308 also reduce the vertical gradient of dissolved ^{231}Pa and ^{230}Th as reversible
309 scavenging act as the vertical transport and increase this vertical transport can
310 decrease the vertical gradient. However, change in the particulate ^{231}Pa and ^{230}Th is
311 small. As stated in Siddall et al., (2005), if we neglect the transport term and the
312 decay term in Eq. (3) and assume particulate phase activity at the surface as 0, when
313 reach equilibrium, the activity of particulate phase will be as in Eq. (7). The
314 particulate phase activity only depends on the production rate, the particle settling
315 velocity and depth. The particulate phase activity will increase linearly with depth
316 and any departure from this linear relationship with depth is due to ocean
317 transport, which is suggested by observations (Bacon and Anderson, 1982; Roy-
318 Barman et al., 1996). Therefore, changing K will have limited influence on
319 particulate phase activity.

$$A_p^i(z) = \frac{\beta^i}{w_s} \cdot z \tag{7}$$

320
321
322 Increasing K will also reduce the spatial gradient in sediment ^{231}Pa/^{230}Th
323 activity ratio and vice versa (Fig. 7). Larger K will decrease the ^{231}Pa and ^{230}Th
324 residence time and most isotopes produced in the water column are removed into
325 sediment locally (Table 2). Therefore, sediment ^{231}Pa/^{230}Th ratio becomes more
326 homogeneous and approaching the production ration of 0.093 (Fig. 7b). The
327 sediment ^{231}Pa/^{230}Th activity ratio in EXP_1 and EXP_2 departures from
328 observations significantly, suggesting the partition coefficient in CTRL is of the right
329 magnitude.

330

331 4.3. Sediment $^{231}Pa/^{230}Th$ ratio in HOSING

332 Potential changes in the export of biogenic particles makes using $^{231}Pa/^{230}Th$
333 ratio to reconstructing AMOC strength under debate. In response to freshwater
334 perturbation in the North Atlantic, both biological productivity and AMOC strength
335 will change and will influence sediment $^{231}Pa/^{230}Th$. Our model with p-fixed and p-
336 coupled ^{231}Pa and ^{230}Th can help detangle these two effects. In this section, we
337 examine the sediment $^{231}Pa/^{230}Th$ (p-fixed and p-coupled) response in the North
338 Atlantic to fresh water perturbation.

339 In HOSING, after applying freshwater forcing to the North Atlantic, AMOC
340 strength quickly decreases to a minimum of 2 Sv (AMOC_off) (Fig. 9a). During the
341 AMOC_off state, compared with CTRL with active AMOC (AMOC_on), p-fixed
342 sediment $^{231}Pa/^{230}Th$ shows an overall increase in the North Atlantic and a decrease
343 in the South Atlantic (Fig. 10b) because of the reduced southward transport of ^{231}Pa
344 from the North Atlantic by AMOC, consistent with paleo proxy evidence there (e.g.
345 Gherardi et al., 2005, 2009; McManus et al., 2004). The overall increase of sediment
346 $^{231}Pa/^{230}Th$ ratio in the North Atlantic in response to AMOC collapse can be seen
347 more clearly in the time evolution of the sediment $^{231}Pa/^{230}Th$ ratio averaged from
348 20°N to 60°N in the North Atlantic (Fig.9b, green). Quantitatively, the $^{231}Pa/^{230}Th$
349 increases from 0.074 in AMOC_on to 0.098 in AMOC_off in the p-fixed version,
350 approaching the production ration of 0.093. This increase of $^{231}Pa/^{230}Th$ is also in
351 the subtropical North Atlantic from the two sites near Bermuda Rise (Fig. 9e and f),
352 which is of comparable magnitude with the change from LGM to HS1 in
353 reconstructions there (McManus et al., 2004). In addition, the pattern of p-fixed
354 (Fig.10a) sediment $^{231}Pa/^{230}Th$ ratio during the Atlantic in AMOC_off state is similar
355 to the opal distribution (Fig.1b) because, without active circulation, sediment
356 $^{231}Pa/^{230}Th$ ratio is more controlled by particle flux effect, which is similar to Pacific
357 in CTRL. It is further noted that our p-fixed sediment $^{231}Pa/^{230}Th$ ratio in HOSING
358 behaves similarly to that in Siddall et al., (2007).

359 The overall increase in p-fixed sediment $^{231}Pa/^{230}Th$ ratio in the North
360 Atlantic is not homogenous and the magnitude of the change between AMOC_on and

AMOC_off varies with location because of the distribution of particle flux, especially opal flux (Fig.9 and 10). The maximum increase in p-fixed sediment $^{231}Pa/^{230}Th$ ratio occurs near 40°N western Atlantic, where the opal production in our model is maximum in North Atlantic (Fig. 1b). The sediment $^{231}Pa/^{230}Th$ ratio in this region during AMOC_on is larger than production ratio of 0.093 because opal maximum provides extra ^{231}Pa to this region ("particle flux effect"), which overwhelms the active ocean circulation transporting ^{231}Pa southward outside this region (Fig. 9d, green). During AMOC_off, without active ocean circulation, the particle flux effect becomes even stronger because less ^{231}Pa is transported out of the North Atlantic and p-fixed sediment $^{231}Pa/^{230}Th$ ratio gets even larger.

Most regions in the Atlantic, p-coupled sediment $^{231}Pa/^{230}Th$ show similar response to p-fixed $^{231}Pa/^{230}Th$ in HOSING. The evolution of p-fixed and p-coupled sediment $^{231}Pa/^{230}Th$ activity ratio in HOSING are highly correlated (Fig. 11a). The change of sediment $^{231}Pa/^{230}Th$ ratio from AMOC_on to AMOC_off are similar in both p-fixed and p-coupled version (Fig.11b). The correlation between p-fixed and p-coupled sediment $^{231}Pa/^{230}Th$ ratio change is 0.72 (1455points) and the linear regression coefficient is 0.71 (R^2 = 0.52). High correlation between p-fixed and p-coupled response mainly happens over low productivity region (Fig.1, 10, and 11), where circulation effect on sediment $^{231}Pa/^{230}Th$ is more important than the particle change in HOSING.

However, the responses of p-fixed and p-coupled sediment $^{231}Pa/^{230}Th$ to the fresh water forcing can differ significantly in high productivity regions because of the change of productivity. With persistent freshwater forcing in the North Atlantic, most regions in the North Atlantic show reduced production of $CaCO_3$, opal and POC (Fig. 8). Productivity in North Atlantic is suggested to be halved during AMOC collapse because of increased stratification, which reduces nutrient supply from deep ocean (Schmittner, 2005). In our model, the productivity in mid-latitude North Atlantic is indeed greatly reduced after the freshwater forcing. For example, opal production from 30°N-50°N in the Atlantic at the end of HOSING is reduced by 50%~90% of its original value in CTRL. However, opal production increases in high latitude North Atlantic at north of 50°N. The pattern of opal production changes

392 with high opal production region shifts northward in HOSING (Fig. 8 d, e and f). The
393 particle flux change will influence sediment $^{231}Pa/^{230}Th$ as discussed below.
394 In subpolar region, the opal productivity increases during AMOC_off and will
395 result an increase in sediment $^{231}Pa/^{230}Th$, which is enhance the increase of
396 sediment $^{231}Pa/^{230}Th$ caused by reduced AMOC. Therefore, the increase in p-coupled
397 sediment $^{231}Pa/^{230}Th$ between AMOC_off and AMOC_on is larger than p-fixed
398 sediment $^{231}Pa/^{230}Th$ (Fig.9c).
399 In the mid-latitude North Atlantic, the opal productivity decreases during
400 AMOC_off and will lead to a decrease in sediment $^{231}Pa/^{230}Th$, which is opposite to
401 the effect of reduced AMOC. Therefore, p-coupled sediment $^{231}Pa/^{230}Th$ shows an
402 initial decrease in first 200 years (Fig.9 d, e, and f, red dash) caused by the reduced
403 opal productivity. But this decrease trend is reversed eventually, suggesting the
404 influence of particle flux change is overwhelmed by the effect of reduced AMOC. It
405 the long run, most regions in the subtropical and mid-latitude Atlantic show
406 increased sediment $^{231}Pa/^{230}Th$ in HOSING, indicating the dominant effect of
407 reduced AMOC. But sediment $^{231}Pa/^{230}Th$ at 40°N west Atlantic, where opal
408 productivity is maximum in AMOC_on, show a decrease from AMOC_on to AMOC_off.
409 During AMOC_on, the opal productivity maximum at 40°N west Atlantic lead to
410 regional maximum sediment $^{231}Pa/^{230}Th$ because of the particle flux effected, which
411 has been explained previously. During AMOC_off, this opal productivity maximum is
412 eliminated and no more extra ^{231}Pa is supplied by surroundings to this region. The
413 decrease in sediment $^{231}Pa/^{230}Th$ caused by productivity change is larger than the
414 increase caused by the reduced AMOC. Therefore, sediment $^{231}Pa/^{230}Th$ experienced
415 a decrease from AMOC_on to AMOC_off. Our results suggest that although the
416 circulation effect is more dominant than the particle change in controlling sediment
417 $^{231}Pa/^{230}Th$ on long time scale in most of North Atlantic, particle flux change can be
418 important on short time scale and in high productivity regions. Therefore, we
419 should be cautious when using sediment $^{231}Pa/^{230}Th$ to reconstruct AMOC
420 variations in the past.
421
422

It is suggested that the particulate $^{231}Pa/^{230}Th$ response to the change of AMOC depends on the location and depth. Above 2km and high latitude North Atlantic, particulate $^{231}Pa/^{230}Th$ decreases with the increased AMOC (Rempfer et al., 2017). Our results are consistent with this finding (Fig. 12 a and b). Both p-fixed and p-coupled particulate $^{231}Pa/^{230}Th$ show similar patterns of change between AMOC_on and AMOC_off: decrease in particulate $^{231}Pa/^{230}Th$ at shallow depth and north of 60°N and increase in particulate $^{231}Pa/^{230}Th$ below 2km and south of 60°N during AMOC_off. Therefore, sediment depth should be taken into consideration when interpreting sediment $^{231}Pa/^{230}Th$. Since the pattern in p-coupled is similar to the pattern in p-fixed, the opposite particulate $^{231}Pa/^{230}Th$ changes in shallow and deep North Atlantic is associated with AMOC. During AMOC_on, upper limb of AMOC (about upper 1km) transport water northward, which provides extra ^{231}Pa to North Atlantic and particulate $^{231}Pa/^{230}Th$ is larger than the production ratio of 0.093. In contrast, the lower limb of AMOC (2km-3km) features southward transport, which transports ^{231}Pa to the Southern Ocean and particulate $^{231}Pa/^{230}Th$ is smaller than the production ratio of 0.093 (Fig. 12 solid). During AMOC_off, ocean transport of 231Pa is greatly reduced. Therefore, shallow (deep) depth experiences a decrease (increase) in particulate $^{231}Pa/^{230}Th$ and the vertical gradient in the particulate $^{231}Pa/^{230}Th$ is also greatly reduced (Fig. 12 c). Our results support that the depth dependence of particulate $^{231}Pa/^{230}Th$ is mainly caused by lateral transport of ^{231}Pa by circulation (Gherardi et al., 2009; Lippold et al., 2011, 2012a; Luo et al., 2010; Rempfer et al., 2017).

Overall, our model is able to simulate the correct magnitude of the sediment $^{231}Pa/^{230}Th$ ratio response to the freshwater forcing. Change of circulation has the dominant influence on sediment $^{231}Pa/^{230}Th$ on long time scale over most of regions in the hosing experiment, although the detailed difference between p-fixed and p-coupled sediment $^{231}Pa/^{230}Th$ ratio response to freshwater forcing in different locations can be complicated.

5. Summary

^{231}Pa and ^{230}Th have been implemented in the ocean model of the CESM in both the p-coupled and p-fixed forms. Our control experiment under present day climate forcing is able to simulate most ^{231}Pa and ^{230}Th water column activity and sediment ^{231}Pa/^{230}Th activity ratio consistent with observations by using the parameters that are suggested by Chase et al., (2002) and used in Siddall et al. (2005). Our sensitivity experiments with varying parameters suggest that these parameters are of the right magnitude.

Furthermore, our model is able to simulate the overall sediment ^{231}Pa/^{230}Th ratio change in the North Atlantic with a magnitude comparable to the reconstruction in response to the collapse of AMOC, although the detailed response can be complicated in different regions. Finally, the p-fixed form is able to capture many major features of that of the p-coupled form over large ocean areas on long time scale, although the two forms can also differ significantly in some regions, especially the region with high opal productivity. Therefore, with both p-fixed and p-coupled ^{231}Pa and ^{230}Th, our model can serve as a useful tool to improve our understanding of the processes of ^{231}Pa and ^{230}Th and also interpretations of sediment ^{231}Pa/^{230}Th reconstructions for past ocean circulation and climate changes.

Code availability:

The ^{231}Pa and ^{230}Th isotope source code of both p-fixed and p-coupled versions for CESM1.3 is included as supplementary material here.

Acknowledgement:

This work is supported by US NSF P2C2 program and the National Science Foundation of China No. 41630527. Computing resources (ark:/85065/d7wd3xhc) were provided by the Climate Simulation Laboratory at NCAR's Computational and Information Systems Laboratory, sponsored by the National Science Foundation and other agencies.

References:

Anderson, R. F., Bacon, M. P. and Brewer, P. G.: Removal of230Th and231Pa from the open ocean, Earth Planet. Sci. Lett., 62(1), 7–23, doi:10.1016/0012-821X(83)90067-5, 1983.

Anderson, R. F., Lao, Y., Broecker, W. S., Trumbore, S. E., Hofmann, H. J. and Wolfli, W.: Boundary scavenging in the Pacific Ocean: A comparison of 10Be and 231Pa, Earth Planet. Sci. Lett., 96(3–4), 287–304, doi:10.1016/j.cognition.2008.05.007, 1990.

Anderson, R. F., Fleisher, M. Q., Biscaye, P. E., Kumar, N., Dittrich, B., Kubik, P. and Suter, M.: Anomalous boundary scavenging in the Middle Atlantic Bight: evidence from 230Th, 231Pa, 10Be and 210Pb, Deep. Res. Part II, 41(2–3), 537–561, doi:10.1016/0967-0645(94)90034-5, 1994.

Armstrong, R. A., Lee, C., Hedges, J. I., Honjo, S. and Wakeham, S. G.: A new, mechanistic model for organic carbon fluxes in the ocean based on the quantitative association of POC with ballast minerals, Deep. Res. Part II Top. Stud. Oceanogr., 49(1–3), 219–236, doi:10.1016/S0967-0645(01)00101-1, 2002.

Arsouze, T., Dutay, J.-C., Lacan, F. and Jeandel, C.: Reconstructing the Nd oceanic cycle using a coupled dynamical – biogeochemical model, Biogeosciences, 6(12), 2829–2846, doi:10.5194/bg-6-2829-2009, 2009.

Bacon, M. and Anderson, R.: Distribution of Thorium Isotopes between dissolved and particulate forms in the deep sea, J. Geophys. Res. …, 87(1), 2045–2056, 1982.

Bacon, M. P. and Rosholt, J. N.: Accumulation rates of 230Th, 231Pa, and some transition metals on the Bermuda Rise, Geochim. Cosmochim. Acta, 46, 651–666, 1982.

Bacon, M. P., Huh, C. A. and Moore, R. M.: Vertical profiles of some natural radionuclides over the Alpha Ridge, Arctic Ocean, Earth Planet. Sci. Lett., 95(1–2), 15–22, doi:10.1016/0012-821X(89)90164-7, 1989.

Bradtmiller, L. I., Anderson, R. F., Fleisher, M. Q. and Burckle, L. H.: Opal burial in the equatorial Atlantic Ocean over the last 30 ka: Implications for glacial-interglacial changes in the ocean silicon cycle, Paleoceanography, 22(4), 1–15, doi:10.1029/2007PA001443, 2007.

Bradtmiller, L. I., McManus, J. F. and Robinson, L. F.: 231Pa/230Th evidence for a weakened but persistent Atlantic meridional overturning circulation during Heinrich Stadial 1, Nat. Commun., 5, 5817, doi:10.1038/ncomms6817, 2014.

Burckel, P., Waelbroeck, C., Luo, Y., Roche, D. M., Pichat, S., Jaccard, S. L., Gherardi, J., Govin, A., Lippold, J. and Thil, F.: Changes in the geometry and strength of the Atlantic meridional overturning circulation during the last glacial (20-50 ka), Clim. Past, 12(11), 2061–2075, doi:10.5194/cp-12-2061-2016, 2016.

Chase, Z. and Robert F, A.: Comment on "On the importance of opal, carbonate, and lithogenic clays in scavenging and fractionating 230Th, 231Pa and 10Be in the ocean" by S. Luo and T.-L. Ku, Earth Planet. Sci. Lett., 220(1–2), 201–211, doi:10.1016/S0012-821X(04)00027-5, 2004.

Chase, Z., Anderson, R. F., Fleisher, M. Q. and Kubik, P. W.: The influence of particle composition and particle flux on scavenging of Th , Pa and Be in the ocean, Earth Planet. Sci. Lett., 204(1–2), 215–229, doi:10.1016/S0012-821X(02)00984-6, 2002.

530 Cochran, J. K., Livingston, H. D., Hirschberg, D. J. and Surprenant, L. D.: Natural and
531 anthropogenic radionuclide distributions in the northwest Atlantic Ocean, Earth
532 Planet. Sci. Lett., 84(2–3), 135–152, doi:10.1016/0012-821X(87)90081-1, 1987.
533 Cochran, J. K., Hirschberg, D. J., Livingston, H. D., Buesseler, K. O. and Key, R. M.:
534 Natural and anthropogenic radionuclide distributions in the Nansen Basin, Artic
535 Ocean: Scavenging rates and circulation timescales, Deep. Res. Part II, 42(6), 1495–
536 1517, doi:10.1016/0967-0645(95)00051-8, 1995.
537 Colley, S., Thomson, J. and Newton, P. P.: Detailed Th-230, Th-232 and Pb-210 fluxes
538 recorded by the 1989/90 BOFS sediment trap time-series at 48N, 20W, Deep - Sea
539 Res. Part I - Oceanogr. Res. Pap., 42(6), 833–848, 1995.
540 Coppola, L., Roy-Barman, M., Mulsow, S., Povinec, P. and Jeandel, C.: Thorium
541 isotopes as tracers of particles dynamics and deep water circulation in the Indian
542 sector of the Southern Ocean (ANTARES IV), Mar. Chem., 100(3–4 SPEC. ISS.), 299–
543 313, doi:10.1016/j.marchem.2005.10.019, 2006.
544 Danabasoglu, G., Bates, S. C., Briegleb, B. P., Jayne, S. R., Jochum, M., Large, W. G.,
545 Peacock, S. and Yeager, S. G.: The CCSM4 ocean component, J. Clim., 25(5), 1361–
546 1389, doi:10.1175/JCLI-D-11-00091.1, 2012.
547 DeMaster, D. J.: The marine budgets of silica and 32Si, Yale., 1979.
548 Deng, F., Thomas, A. L., Rijkenberg, M. J. A. and Henderson, G. M.: Controls on
549 seawater 231Pa, 230Th and 232Th concentrations along the flow paths of deep
550 waters in the Southwest Atlantic, Earth Planet. Sci. Lett., 390, 93–102,
551 doi:10.1016/j.epsl.2013.12.038, 2014.
552 Doney, S. C., Lima, I., Feely, R. A., Glover, D. M., Lindsay, K., Mahowald, N., Moore, J. K.
553 and Wanninkhof, R.: Mechanisms governing interannual variability in upper-ocean
554 inorganic carbon system and air-sea CO2 fluxes: Physical climate and atmospheric
555 dust, Deep. Res. Part II Top. Stud. Oceanogr., 56(8–10), 640–655,
556 doi:10.1016/j.dsr2.2008.12.006, 2009.
557 Dutay, J.-C., Lacan, F., Roy-Barman, M. and Bopp, L.: Influence of particle size and
558 type on 231 Pa and 230 Th simulation with a global coupled biogeochemical-ocean
559 general circulation model: A first approach, Geochemistry, Geophys. Geosystems,
560 10(1), doi:10.1029/2008GC002291, 2009.
561 Edmonds, H. N., Moran, S. B., Hoff, J. A., Smith, J. N. and Edwards, R. L.: Protactinium-
562 231 and Thorium-230 Abundances and High Scavenging Rates in the Western Arctic
563 Ocean, Science (80-.)., 280(5362), 405–407, doi:10.1126/science.280.5362.405,
564 1998.
565 Edmonds, H. N., Moran, S. B., Cheng, H. and Edwards, R. L.: 230Th and 231Pa in the
566 Arctic Ocean: Implications for particle fluxes and basin-scale Th/Pa fractionation,
567 Earth Planet. Sci. Lett., 227(1–2), 155–167, doi:10.1016/j.epsl.2004.08.008, 2004.
568 Francois, R., Bacon, M. P., Altabet, M. A. and Labeyrie, L. D.: Glacial/interglacial
569 changes in sediment rain rate in the SW Indian Sector of subantarctic Waters as
570 recorded by 230Th, 231Pa, U, and d15N, Paleoceanography, 8(5), 611–629,
571 doi:10.1029/93PA00784, 1993.
572 Frank, M.: Reconstruction of Late Quaternary environmental conditions applying the
573 natural radionuclides 230Th, 10Be, 231Pa and 238U: A study of deep-sea sediments
574 from the eastern sector of the Antarctic Circumpolar Current System, Alfred
575 Wegener Institute for Polar and Marine Research., 1996.

576 Frank, M., Eisenhauer, A., Kubik, P. W., Dittrich-hannen, B. and Segl, M.: Beryllium 10,
577 thorium 230, and protactinium 231 in Galapagos microplate sediments:
578 Implications of hydrothermal activity and paleoproductivity changes during the last
579 100,000 years, Palaeogeography, 9(4), 559–578, 1994.
580 Geibert, W. and Usbeck, R.: Adsorption of thorium and protactinium onto different
581 particle types: Experimental findings, Geochim. Cosmochim. Acta, 68(7), 1489–
582 1501, doi:10.1016/j.gca.2003.10.011, 2004.
583 Gherardi, J., Labeyrie, L., Mcmanus, J., Francois, R., Skinner, L. and Cortijo, E.:
584 Evidence from the Northeastern Atlantic basin for variability in the rate of the
585 meridional overturning circulation through the last deglaciation, Earth Planet. Sci.
586 Lett., 240(3–4), 710–723, doi:10.1016/j.epsl.2005.09.061, 2005.
587 Gherardi, J.-M., Labeyrie, L., Nave, S., Francois, R., McManus, J. F. and Cortijo, E.:
588 Glacial-interglacial circulation changes inferred from 231 Pa/ 230 Th sedimentary
589 record in the North Atlantic region, Paleoceanography, 24(2),
590 doi:10.1029/2008PA001696, 2009.
591 Guo, L., Santschi, P. H., Baskaran, M. and Zindler, A.: Distribution of dissolved and
592 particulate 230Th and 232Th in seawater from the Gulf of Mexico and off Cape
593 Hatteras as measured by SIMS, Earth Planet. Sci. Lett., 133(1), 117–128, 1995.
594 Gutjahr, M., Frank, M., Stirling, C. H., Keigwin, L. D. and Halliday, a. N.: Tracing the Nd
595 isotope evolution of North Atlantic Deep and Intermediate Waters in the western
596 North Atlantic since the Last Glacial Maximum from Blake Ridge sediments, Earth
597 Planet. Sci. Lett., 266(1–2), 61–77, doi:10.1016/j.epsl.2007.10.037, 2008.
598 Hall, I. R., Moran, S. B., Zahn, R., Knutz, P. C., Shen, C.-C. and Edwards, R. L.:
599 Accelerated drawdown of meridional overturning in the late-glacial Atlantic
600 triggered by transient pre-H event freshwater perturbation, Geophys. Res. Lett.,
601 33(16), L16616, doi:10.1029/2006GL026239, 2006.
602 Hayes, C. T., Anderson, R. F., Fleisher, M. Q., Serno, S., Winckler, G. and Gersonde, R.:
603 Quantifying lithogenic inputs to the North Pacific Ocean using the long-lived
604 thorium isotopes, Earth Planet. Sci. Lett., 383, 16–25,
605 doi:10.1016/j.epsl.2013.09.025, 2013.
606 Hayes, C. T., Anderson, R. F., Fleisher, M. Q., Huang, K. F., Robinson, L. F., Lu, Y.,
607 Cheng, H., Edwards, R. L. and Moran, S. B.: ^{230}Th and ^{231}Pa on GEOTRACES GA03, the
608 U.S. GEOTRACES North Atlantic transect, and implications for modern and
609 paleoceanographic chemical fluxes, Deep. Res. Part II Top. Stud. Oceanogr., 116, 29–
610 41, doi:10.1016/j.dsr2.2014.07.007, 2015.
611 Henderson, G. M. and Anderson, R. F.: The U-series toolbox for paleoceanography,
612 Rev. Mineral. Geochemistry, 52(1), 493–531, doi:10.2113/0520493, 2003.
613 Henderson, G. M., Heinze, C., Anderson, R. F. and Winguth, A. M. E.: Global
614 distribution of the 230Th flux to ocean sediments constrained by GCM modelling,
615 Deep. Res. Part I Oceanogr. Res. Pap., 46(11), 1861–1893, doi:10.1016/S0967-
616 0637(99)00030-8, 1999.
617 Hoffmann, S. S., McManus, J. F., Curry, W. B. and Brown-Leger, L. S.: Persistent export
618 of 231Pa from the deep central Arctic Ocean over the past 35,000 years., Nature,
619 497(7451), 603–6, doi:10.1038/nature12145, 2013.
620 Hsieh, Y. Te, Henderson, G. M. and Thomas, A. L.: Combining seawater 232Th and
621 230Th concentrations to determine dust fluxes to the surface ocean, Earth Planet.

622 Sci. Lett., 312(3–4), 280–290, doi:10.1016/j.epsl.2011.10.022, 2011.
623 Huh, C. A. and Beasley, T. M.: Profiles of dissolved and particulate thorium isotopes
624 in the water column of coastal Southern California, Earth Planet. Sci. Lett., 85(1–3),
625 1–10, doi:10.1016/0012-821X(87)90016-1, 1987.
626 Hurrell, J. W., Holland, M. M., Gent, P. R., Ghan, S., Kay, J. E., Kushner, P. J., Lamarque, J.
627 F., Large, W. G., Lawrence, D., Lindsay, K., Lipscomb, W. H., Long, M. C., Mahowald, N.,
628 Marsh, D. R., Neale, R. B., Rasch, P., Vavrus, S., Vertenstein, M., Bader, D., Collins, W.
629 D., Hack, J. J., Kiehl, J. and Marshall, S.: The community earth system model: A
630 framework for collaborative research, Bull. Am. Meteorol. Soc., 94(9), 1339–1360,
631 doi:10.1175/BAMS-D-12-00121.1, 2013.
632 Jahn, A., Lindsay, K., Giraud, X., Gruber, N., Otto-Bliesner, B. L., Liu, Z. and Brady, E. C.:
633 Carbon isotopes in the ocean model of the Community Earth System Model
634 (CESM1), Geosci. Model Dev., 8(8), 2419–2434, doi:10.5194/gmd-8-2419-2015,
635 2015.
636 Jonkers, L., Zahn, R., Thomas, A., Henderson, G., Abouchami, W., Fran??ois, R.,
637 Masque, P., Hall, I. R. and Bickert, T.: Deep circulation changes in the central South
638 Atlantic during the past 145 kyrs reflected in a combined 231Pa/230Th,
639 Neodymium isotope and benthic dC13 record, Earth Planet. Sci. Lett., 419, 14–21,
640 doi:10.1016/j.epsl.2015.03.004, 2015.
641 Keigwin, L. D. and Boyle, E. A.: Did North Atlantic overturning halt 17,000 years
642 ago?, Paleoceanography, 23(1), 1–5, doi:10.1029/2007PA001500, 2008.
643 Kriest, I.: Different parameterizations of marine snow in a 1D-model and their
644 influence on representation of marine snow, nitrogen budget and sedimentation,
645 Deep. Res. Part I Oceanogr. Res. Pap., 49(12), 2133–2162, doi:10.1016/S0967-
646 0637(02)00127-9, 2002.
647 Ku, T. L.: Uranium series disequilibrium in deep sea sediments, Columbia., 1966.
648 Ku, T. L., Bischoff, J. L. and Boersma, A.: Age studies of Mid-Atlantic Ridge sediments
649 near 42??N and 20??N, Deep. Res. Oceanogr. Abstr., 19(3), 233–247,
650 doi:10.1016/0011-7471(72)90033-2, 1972.
651 Kumar, N.: Trace metals and natural radionuclides as tracers of ocean productivity,
652 Columbia., 1994.
653 Kumar, N., Gwiazda, R., Anderson, R. F. and Froelich, P. N.: 231Pa/230Th ratios in
654 sediments as a proxy for past changes in Southern Ocean productivity, Nature, 362,
655 45–48, doi:10.1038/362045a0, 1993.
656 Large, W. G. and Yeager, S. G.: The global climatology of an interannually varying air–
657 sea flux data set, Clim. Dyn., 33(2–3), 341–364, doi:10.1007/s00382-008-0441-3,
658 2008.
659 Lippold, J., Grützner, J., Winter, D., Lahaye, Y., Mangini, A. and Christi, M.: Does
660 sedimentary 231Pa/230Th from the Bermuda Rise monitor past Atlantic Meridional
661 Overturning Circulation?, Geophys. Res. Lett., 36(12), 1–6,
662 doi:10.1029/2009GL038068, 2009.
663 Lippold, J., Gherardi, J. M. and Luo, Y.: Testing the $^{231}Pa/^{230}Th$ paleocirculation proxy:
664 A data versus 2D model comparison, Geophys. Res. Lett., 38(20), 1–7,
665 doi:10.1029/2011GL049282, 2011.
666 Lippold, J., Mulitza, S., Mollenhauer, G., Weyer, S., Heslop, D. and Christl, M.:
667 Boundary scavenging at the East Atlantic margin does not negate use of 231Pa/

668 230Th to trace Atlantic overturning, Earth Planet. Sci. Lett., 333–334, 317–331,
669 doi:10.1016/j.epsl.2012.04.005, 2012a.
670 Lippold, J., Luo, Y., Francois, R., Allen, S. E., Gherardi, J., Pichat, S., Hickey, B. and
671 Schulz, H.: Strength and geometry of the glacial Atlantic Meridional Overturning
672 Circulation, Nat. Geosci., 5(11), 813–816, doi:10.1038/ngeo1608, 2012b.
673 Long, M. C., Lindsay, K., Peacock, S., Moore, J. K. and Doney, S. C.: Twentieth-century
674 oceanic carbon uptake and storage in CESM1(BGC), J. Clim., 26(18), 6775–6800,
675 doi:10.1175/JCLI-D-12-00184.s1, 2013.
676 Luo, S. and Ku, T. L.: Oceanic 231Pa/230Th ratio influenced by particle composition
677 and remineralization, Earth Planet. Sci. Lett., 167(3–4), 183–195,
678 doi:10.1016/S0012-821X(99)00035-7, 1999.
679 Luo, S. D., Ku, T. L., Kusakabe, M., Bishop, J. K. B. and Yang, Y. L.: Tracing particle
680 cycling in the upper ocean with Th-230 and Th-228: An investigation in the
681 equatorial Pacific along 140 degrees W, Deep - Sea Res. Part II - Top. Stud.
682 Oceanogr., 42(2–3), 805–829, doi:10.1016/0967-0645(95)00019-M, 1995.
683 Luo, Y., Francois, R. and Allen, S.: Sediment 231Pa/230Th as a recorder of the rate of
684 the Atlantic meridional overturning circulation: insights from a 2-D model, Ocean
685 Sci., 6(3), 381–400, doi:10.5194/os-6-381-2010, 2010.
686 Mangini, A. and Diester-Hass, L.: Excess Th-230 in sediments off NW Africa traces
687 upwelling during the past 130,000 years, in Coastal upwelling: Its sedimentary
688 records, edited by E. Suess and J. Thiede, pp. 455–470, Plenum., 1983.
689 Mangini, A. and Key, R. M.: A 230Th profile in the Atlantic Ocean, Earth Planet. Sci.
690 Lett., 62(3), 377–384, doi:10.1016/0012-821X(83)90008-0, 1983.
691 Mangini, A. and Sonntag, C.: 231Pa dating of deep-sea cores via 227Th counting,
692 Earth Planet. Sci. Lett., 37(2), 251–256, 1977.
693 Mangini, A. and U., K.: Depositional history in the Clarion-Clipperton zone during the
694 last 250,000 years: 230Th and 231Pa methods, Geol. Jahrb., 87, 105–121, 1987.
695 Marchal, O., François, R., Stocker, T. F. and Joos, F.: Ocean thermohaline circulation
696 and sedimentary 231Pa/230Th ratio, Paleoceanography, 15(6), 625–641 [online]
697 Available from: http://onlinelibrary.wiley.com/doi/10.1029/2000PA000496/full
698 (Accessed 19 April 2016), 2000.
699 McManus, J., Francois, R. and Gherardi, J.: Collapse and rapid resumption of Atlantic
700 meridional circulation linked to deglacial climate changes, Nature, 428(6985), 834–
701 837, 2004.
702 Moore, J. K. and Braucher, O.: Sedimentary and mineral dust sources of dissolved
703 iron to the World Ocean, Biogeosciences, 5(1994), 631–656, doi:10.5194/bgd-4-
704 1279-2007, 2008.
705 Moore, J. K., Doney, S. C., Glover, D. M. and Fung, I. Y.: Iron cycling and nutrient-
706 limitation patterns in surface waters of the World Ocean, , 49, 463–507, 2002.
707 Moore, J. K., Doney, S. C. and Lindsay, K.: Upper ocean ecosystem dynamics and iron
708 cycling in a global three-dimensional model, Global Biogeochem. Cycles, 18(4),
709 doi:10.1029/2004GB002220, 2004.
710 Moore, J. K., Lindsay, K., Doney, S. C., Long, M. C. and Misumi, K.: Marine Ecosystem
711 Dynamics and Biogeochemical Cycling in the Community Earth System Model
712 [CESM1(BGC)]: Comparison of the 1990s with the 2090s under the RCP4.5 and
713 RCP8.5 Scenarios, J. Clim., 26(23), 9291–9312, doi:10.1175/JCLI-D-12-00566.1,

2013.
Moore, R. M. and Hunter, K. A.: Thorium adsorption in the ocean: reversibility and distribution amongst particle sizes, Geochim. Cosmochim. Acta, 49(11), 2253–2257, doi:10.1016/0016-7037(85)90225-X, 1985.
Moore, W. S.: The thorium isotope content of ocean water, Earth Planet. Sci. Lett., 53(3), 419–426, doi:10.1016/0012-821X(81)90046-7, 1981.
Moran, S. B., Hoff, J. A., Buesseler, K. O. and Edwards, R. L.: High precision 230Th and 232Th in the Norwegian Sea and Denmark by thermal ionization mass spectrometry, , 22(19), 2589–2592, 1995.
Moran, S. B., Charette, M. a., Hoff, J. a., Edwards, R. L. and Landing, W. M.: Distribution of 230Th in the Labrador Sea and its relation to ventilation, Earth Planet. Sci. Lett., 150, 151–160, doi:10.1016/S0012-821X(97)00081-2, 1997.
Moran, S. B., Shen, C.-C., Weinstein, S. E., Hettinger, L. H., Hoff, J. H., E dmonds, H. N. and Edwards, R. L.: Constraints on deep water age and particle flux in the Equatorial and South Atlantic Ocean based on seawater 231Pa and 230Th data, Geophys. Res. Lett., 28(18), 3437–3440 [online] Available from: papers2://publication/uuid/2A811583-B32B-4BD8-B582-EC8B0D96A949, 2001.
Moran, S. B., Shen, C. C., Edmonds, H. N., Weinstein, S. E., Smith, J. N. and Edwards, R. L.: Dissolved and particulate 231Pa and 230Th in the Atlantic Ocean: Constraints on intermediate/deep water age, boundary scavenging, and 231Pa/230Th fractionation, Earth Planet. Sci. Lett., 203(3–4), 999–1014, doi:10.1016/S0012-821X(02)00928-7, 2002.
Müller, P. J. and Mangini, A.: Organic carbon decomposition rates in sediments of the pacific manganese nodule belt dated by 230Th and 231Pa, Earth Planet. Sci. Lett., 51(1), 94–114, doi:10.1016/0012-821X(80)90259-9, 1980.
Negre, C., Zahn, R., Thomas, A. L., Masqué, P., Henderson, G. M., Martínez-Méndez, G., Hall, I. R. and Mas, J. L.: Reversed flow of Atlantic deep water during the Last Glacial Maximum., Nature, 468(7320), 84–88, doi:10.1038/nature09508, 2010.
Nozaki, Y. and Horibe, Y.: Alpha-emitting thorium isotopes in northwest Pacific deep waters, Earth Planet. Sci. Lett., 65(1), 39–50, doi:10.1016/0012-821X(83)90188-7, 1983.
Nozaki, Y. and Nakanishi, T.: 231Pa and 230Th profiles in the open ocean water column, Deep Sea Res. Part A, Oceanogr. Res. Pap., 32(10), 1209–1220, doi:10.1016/0198-0149(85)90004-4, 1985.
Nozaki, Y. and Yamada, M.: Thorium and protactinium isotope distributions in waters of the Japan Sea, Deep Sea Res. Part A, Oceanogr. Res. Pap., 34(8), 1417–1430, 1987.
Nozaki, Y. and Yang, H. S.: Th and Pa isotopes in the waters of the western margin of the pacific near Japan: Evidence for release of228Ra and227Ac from slope sediments, J. Oceanogr. Soc. Japan, 43(4), 217–227, doi:10.1007/BF02109817, 1987.
Nozaki, Y., Horibe, Y. and Tsubota, H.: The water column distribution of thorium isotopes in the western North Pacific, Earth Planet. Sci. Lett., 54(54), 203–216, 1981.
Nozaki, Y., Yang, H.-S. and Yamada, M.: Scavenging of thorium in the ocean, J. Geophys. Res., 92(C1), 772, doi:10.1029/JC092iC01p00772, 1987.
Okubo, A., Obata, H., Nozaki, Y., Yamamoto, Y. and Minami, H.: 230Th in the Andaman Sea: Rapid deep-sea renewal, Geophys. Res. Lett., 31(22), 1–5,

760 doi:10.1029/2004GL020226, 2004.
761 Okubo, A., Obata, H., Luo, S., Gamo, T., Yamamoto, Y., Minami, H. and Yamada, M.:
762 Particle flux in the twilight zone of the eastern Indian Ocean: A constraint from
763 234U-230Th and 228Ra-228Th disequilibria, Deep. Res. Part I Oceanogr. Res. Pap.,
764 54(10), 1758–1772, doi:10.1016/j.dsr.2007.06.009, 2007a.
765 Okubo, A., Obata, H., Gamo, T., Minami, H. and Yamada, M.: Scavenging of 230Th in
766 the Sulu Sea, Deep. Res. Part II Top. Stud. Oceanogr., 54(1–2), 50–59,
767 doi:10.1016/j.dsr2.2006.02.016, 2007b.
768 Okubo, A., Obata, H., Gamo, T. and Yamada, M.: 230Th and 232Th distributions in
769 mid-latitudes of the North Pacific Ocean: Effect of bottom scavenging, Earth Planet.
770 Sci. Lett., 339–340, 139–150, doi:10.1016/j.epsl.2012.05.012, 2012.
771 Rempfer, J., Stocker, T. F., Joos, F., Dutay, J.-C. and Siddall, M.: Modelling Nd-isotopes
772 with a coarse resolution ocean circulation model: Sensitivities to model parameters
773 and source/sink distributions, Geochim. Cosmochim. Acta, 75(20), 5927–5950,
774 doi:10.1016/j.gca.2011.07.044, 2011.
775 Rempfer, J., Stocker, T. F., Joos, F., Lippold, J. and Jaccard, S. L.: New insights into
776 cycling of 231 Pa and 230 Th in the Atlantic Ocean, Earth Planet. Sci. Lett., 468, 27–
777 37, doi:10.1016/j.epsl.2017.03.027, 2017.
778 Roberts, N. L., McManus, J. F., Piotrowski, A. M. and McCave, I. N.: Advection and
779 scavenging controls of Pa/Th in the northern NE Atlantic, Paleoceanography, 29(6),
780 668–679, doi:10.1002/2014PA002633, 2014.
781 Robinson, L. F., Belshaw, N. S. and Henderson, G. M.: U and Th concentrations and
782 isotope ratios in modern carbonates and waters from the Bahamas, Geochim.
783 Cosmochim. Acta, 68(8), 1777–1789, doi:10.1016/j.gca.2003.10.005, 2004.
784 Roy-Barman, M., Chen, J. H. and Wasserburg, G. J.: 230Th-232Th systematics in the
785 central Pacific Ocean: The sources and the fates of thorium, Earth Planet. Sci. Lett.,
786 139(3–4), 351–363, doi:10.1016/0012-821X(96)00017-9, 1996.
787 Rutgers van der Loeff, M. M. and Berger, G. W.: Scavenging of 230Th and 231Pa near
788 the antarctic polar front in the South Atlantic, Deep. Res. Part I, 40(2), 339–357,
789 doi:10.1016/0967-0637(93)90007-P, 1993.
790 Schmittner, A.: Decline of the marine ecosystem caused by a reduction in the
791 Atlantic overturning circulation., Nature, 434(7033), 628–633,
792 doi:10.1038/nature03476, 2005.
793 Schmitz, W., Mangini, A., Stoffers, P., Glasby, G. P. and Pluger, W. L.: Sediment
794 accumulation rates in the southwestern Pacific Basin and Aitutaki Passage, Mar.
795 Geol., 73(1), 181–190, 1986.
796 Scholten, J. C., Rutgers van der Loeff, M. M. and Michel, A.: Distribution of 230Th and
797 231Pa in the water column in relation to the ventilation of the deep Arctic basins,
798 Deep. Res. Part II, 42(6), 1519–1531, doi:10.1016/0967-0645(95)00052-6, 1995.
799 Scholten, J. C., Fietzke, J., Mangini, A., Garbe-Schönberg, C. D., Eisenhauer, A.,
800 Schneider, R. and Stoffers, P.: Advection and scavenging: Effects on 230Th and
801 231Pa distribution off Southwest Africa, Earth Planet. Sci. Lett., 271(1–4), 159–169,
802 doi:10.1016/j.epsl.2008.03.060, 2008.
803 Shimmield, G. B. and Price, N. B.: The scavenging of U,230Th and 231Pa during
804 pulsed hydrothermal activity at 20??S, East Pacific Rise, Geochim. Cosmochim. Acta,
805 52(3), 669–677, doi:10.1016/0016-7037(88)90329-8, 1988.

806 Shimmield, G. B., Murray, J. W., Thomson, J., Bacon, M. P., Anderson, R. F. and Price, N.
807 B.: The distribution and behaviour of 230Th and 231Pa at an ocean margin, Baja
808 California, Mexico, Geochim. Cosmochim. Acta, 50(11), 2499–2507,
809 doi:10.1016/0016-7037(86)90032-3, 1986.
810 Siddall, M., Henderson, G. M., Edwards, N. R., Frank, M., Müller, S. a., Stocker, T. F. and
811 Joos, F.: 231Pa/230Th fractionation by ocean transport, biogenic particle flux and
812 particle type, Earth Planet. Sci. Lett., 237(1–2), 135–155,
813 doi:10.1016/j.epsl.2005.05.031, 2005.
814 Siddall, M., Stocker, T. F., Henderson, G. M., Joos, F., Frank, M., Edwards, N. R., Ritz, S.
815 P. and Müller, S. a.: Modeling the relationship between 231 Pa/ 230 Th distribution
816 in North Atlantic sediment and Atlantic meridional overturning circulation,
817 Paleoceanography, 22(2), n/a-n/a, doi:10.1029/2006PA001358, 2007.
818 Thomas, A. L., Henderson, G. M. and Robinson, L. F.: Interpretation of the
819 231Pa/230Th paleocirculation proxy: New water-column measurements from the
820 southwest Indian Ocean, Earth Planet. Sci. Lett., 241(3–4), 493–504,
821 doi:10.1016/j.epsl.2005.11.031, 2006.
822 Trimble, S. M., Baskaran, M. and Porcelli, D.: Scavenging of thorium isotopes in the
823 Canada Basin of the Arctic Ocean, Earth Planet. Sci. Lett., 222(3–4), 915–932,
824 doi:10.1016/j.epsl.2004.03.027, 2004.
825 Venchiarutti, C., van der Loeff, M. R. and Stimac, I.: Scavenging of 231Pa and thorium
826 isotopes based on dissolved and size-fractionated particulate distributions at Drake
827 Passage (ANTXXIV-3), Deep. Res. Part II Top. Stud. Oceanogr., 58(25–26), 2767–
828 2784, doi:10.1016/j.dsr2.2010.10.040, 2011.
829 Vogler, S., Scholten, J., Rutgers van der Loeff, M. M. and Mangini, A.: 230Th in the
830 eastern North Atlantic: the importance of water mass ventilation in the balance of
831 230Th, Earth Planet. Sci. Lett., 156(1–2), 61–74, doi:10.1016/S0012-
832 821X(98)00011-9, 1998.
833 Walter, H. J., Rutgers van der Loeff, M. M. and Hoeltzen, H.: Enhanced scavenging of
834 231Pa relative to 230Th in the South Atlantic south of the Polar Front: Implications
835 for the use of the 231Pa/230Th ratio as a paleoproductivity proxy, Earth Planet. Sci.
836 Lett., 149(1), 85–100, doi:10.1016/S0012-821X(97)00068-X, 1997.
837 Yang, H. S., Nozaki, Y., Sakai, H. and Masuda, A.: The distribution of 230Th and 231Pa
838 in the deep-sea surface sediments of the Pacific Ocean, Geochim. Cosmochim. Acta,
839 50(1), 81–89, doi:10.1016/0016-7037(86)90050-5, 1986.
840 Yong-Liang Yang, Elderfield, H., Pedersen, T. F. and Ivanovich, M.: Geochemical
841 record of the Panama Basin during the Last Glacial Maximum carbon event shows
842 that the glacial ocean was not suboxic, Geology, 23(12), 1115–1118,
843 doi:10.1130/0091-7613(1995)023<1115:GROTPB>2.3.CO, 1995.
844 Yong Lao, Anderson, R. F., Broecker, W. S., Trumbore, S. E., Hofmann, H. J. and Wolfli,
845 W.: Transport and burial rates of 10Be and 231Pa in the Pacific Ocean during the
846 Holocene period, Earth Planet. Sci. Lett., 113(1–2), 173–189, doi:10.1016/0012-
847 821X(92)90218-K, 1992.
848 Yu, E.-F.: Variations in the Particulate Flux of 230Th and 231Pa and
849 Paleoceanographic Applications of the 231Pa/230Th Ratio, WHOI/MIT., 1994.
850 Yu, E.-F., Francois, R. and Bacon, M. P.: Similar rates of modern and last-glacial ocean
851 thermohaline circulation inferred from radiochemical data, Nature, 379(6567),

852 689–694, doi:10.1038/379689a0, 1996.
853

Variable	Symbol	Value	Units
Production of ^{231}Pa from U decay	β^{Pa}	$2.33*10^{-3}$	dpm m^{-3} yr^{-1}
Production of ^{230}Th from U decay	β^{Th}	$2.52*10^{-2}$	dpm m^{-3} yr^{-1}
Decay constant of ^{231}Pa	λ^{Pa}	$2.13*10^{-5}$	yr^{-1}
Decay constant of ^{230}Th	λ^{Th}	$9.22*10^{-6}$	yr^{-1}
Index for ^{231}Pa and ^{230}Th	i		
Index for particle type	j		
Total isotope activity	A_t		dpm m^{-3}
Dissolved isotope activity	A_d		dpm m^{-3}
Particle associated activity	A_p		dpm m^{-3}
Particle settling velocity	w_s	1000	m yr^{-1}
Particle concentration	C		kg m^{-3}
Density of seawater		1024.5	kg m^{-3}
Ratio between particle concentration and density of seawater	R		

Table 1. List of parameters, abbreviations and values.

	CTRL		EXP_1		EXP_2	
	^{231}Pa	^{230}Th	^{231}Pa	^{230}Th	^{231}Pa	^{230}Th
K_{CaCO_3}	$2.5*10^5$	$1.0*10^7$	$5*10^4$	$2*10^6$	$1.25*10^6$	$5*10^7$
K_{opal}	$1.67*10^6$	$5*10^5$	$3.33*10^5$	$1*10^5$	$8.33*10^6$	$2.5*10^6$
K_{POC}	$1.0*10^7$	$1.0*10^7$	$2*10^6$	$2*10^6$	$5*10^7$	$5*10^7$
T(yr)	118	33	501	143	27	9

Table 2. Partition coefficients for different particle types and residence time for ^{231}Pa and ^{230}Th in different experiments. Partition coefficients used in CTRL follows (Chase et al., 2002; Siddall et al., 2005)

WATER COLUMN ACTIVITY	**Holocene core-top ^{231}Pa/^{230}Th**
(Guo et al., 1995)	(Yu, 1994)
(Cochran et al., 1987)	(DeMaster, 1979)
(Nozaki et al., 1987)	(Bacon and Rosholt, 1982)
(Bacon and Anderson, 1982)	(Mangini and Diester-Hass, 1983)
(Bacon et al., 1989)	(Kumar, 1994)
(Huh and Beasley, 1987)	(Yang et al., 1986)
(Rutgers van der Loeff and Berger, 1993)	(Anderson et al., 1983)
(Nozaki et al., 1981)	(Anderson et al., 1994)
(Nozaki and Nakanishi, 1985)	(Ku, 1966)
(Mangini and Key, 1983)	(Ku et al., 1972)

(Nozaki and Horibe, 1983)	(Frank et al., 1994)
(Moore, 1981)	(Shimmield et al., 1986)
(Nozaki and Yamada, 1987)	(Frank, 1996)
(Roy-Barman et al., 1996)	(Yong Lao et al., 1992)
(Nozaki and Yang, 1987)	(Francois et al., 1993)
(Moran et al., 1995)	(Anderson et al., 1990)
(Luo et al., 1995)	(Mangini and Sonntag, 1977)
(Colley et al., 1995)	(Schmitz et al., 1986)
(Scholten et al., 1995)	(Shimmield and Price, 1988)
(Cochran et al., 1995)	(Yong-Liang Yang et al., 1995)
(Vogler et al., 1998)	(Müller and Mangini, 1980)
(Moran et al., 1997)	(Mangini and U., 1987)
(Edmonds et al., 1998)	(Scholten et al., 1995)
(Moran et al., 2001)	(Walter et al., 1997)
(Edmonds et al., 2004)	(Lippold et al., 2011)
(Okubo et al., 2007b)	(Lippold et al., 2012b)
(Coppola et al., 2006)	(Bradtmiller et al., 2007)
(Moran et al., 2002)	(Gherardi et al., 2005)
(Okubo et al., 2004)	(Gutjahr et al., 2008)
(Okubo et al., 2007a)	(Hall et al., 2006)
(Okubo et al., 2012)	(Lippold et al., 2011)
(Robinson et al., 2004)	(Roberts et al., 2014)
(Thomas et al., 2006)	(Bradtmiller et al., 2014)
(Trimble et al., 2004)	(Burckel et al., 2016)
(Venchiarutti et al., 2011)	(Hoffmann et al., 2013)
(Hsieh et al., 2011)	(Jonkers et al., 2015)
(Scholten et al., 2008)	(Negre et al., 2010)
(Luo et al., 2010)	
(Deng et al., 2014)	
(Hayes et al., 2013)	
(Hayes et al., 2015)	

Table 3. References for observations of water column ^{231}Pa and ^{230}Th activity and Holocene core-top $^{231}Pa/^{230}Th$.

Figures:

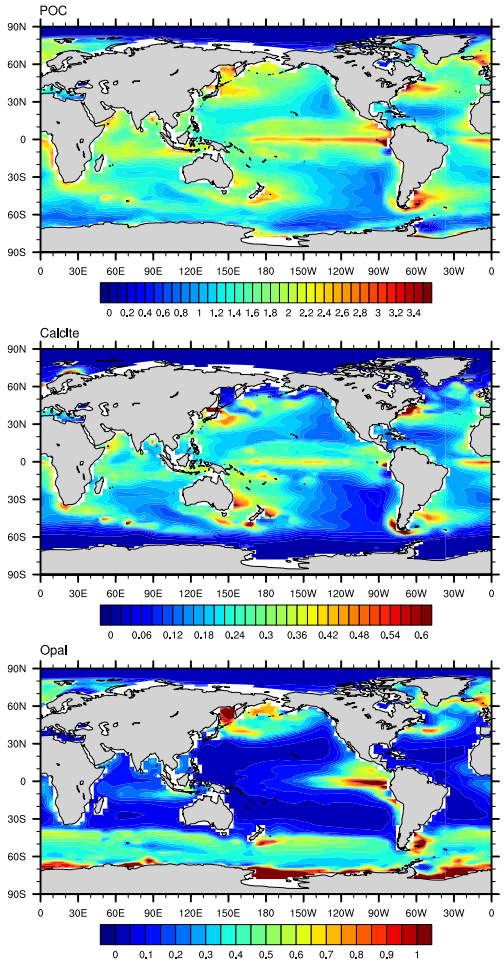

886

887 Figure 1. Annual mean particle fluxes in CESM. (a) $CaCO_3$ flux at 105m (mol m^{-2} yr^{-1}).

888 (b) Opal flux at 105m (mol m^{-2} yr^{-1}). (c) POC flux at 105m (mol m^{-2} yr^{-1}).

889

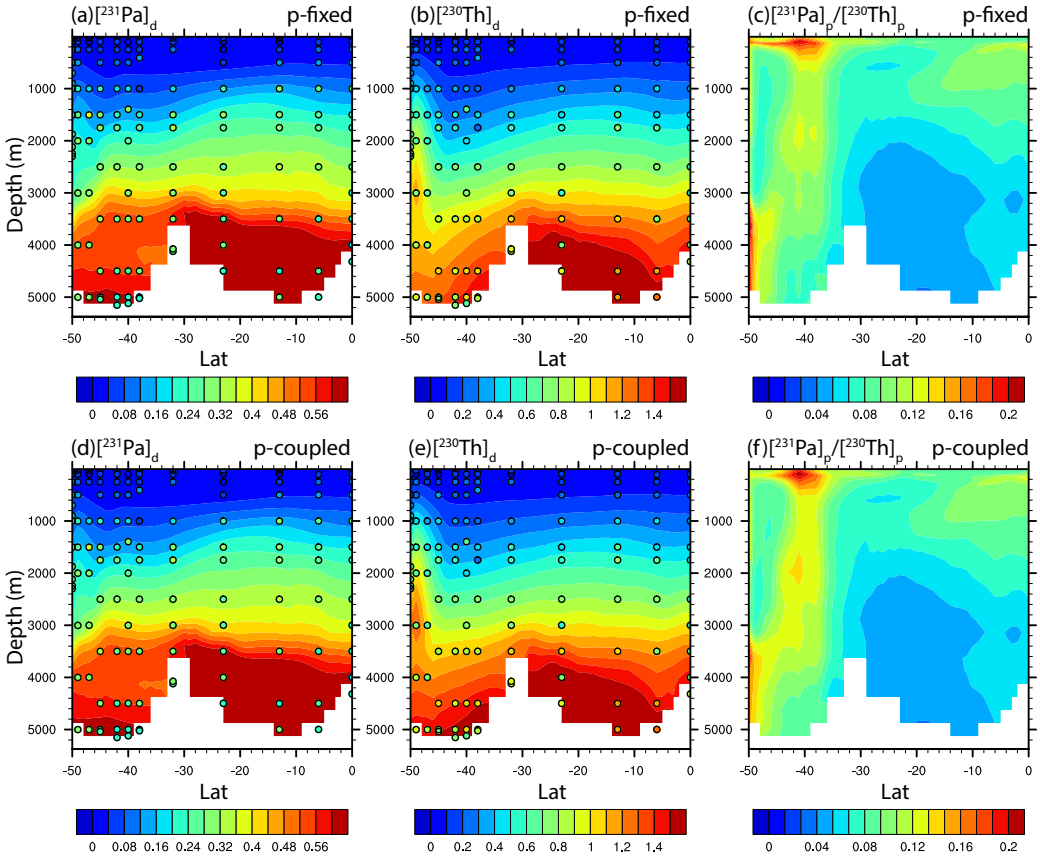

Figure 2. Dissolved ^{231}Pa, dissolved ^{230}Th and particulate ^{231}Pa/^{230}Th in CTRL along GEOTRACES transect GA02S (Deng et al., 2014) (the track is indicated in Fig. S4) for both p-fixed and p-coupled ^{231}Pa and ^{230}Th. Observations of dissolved ^{231}Pa and ^{230}Th activity are superimposed using the same colormap.

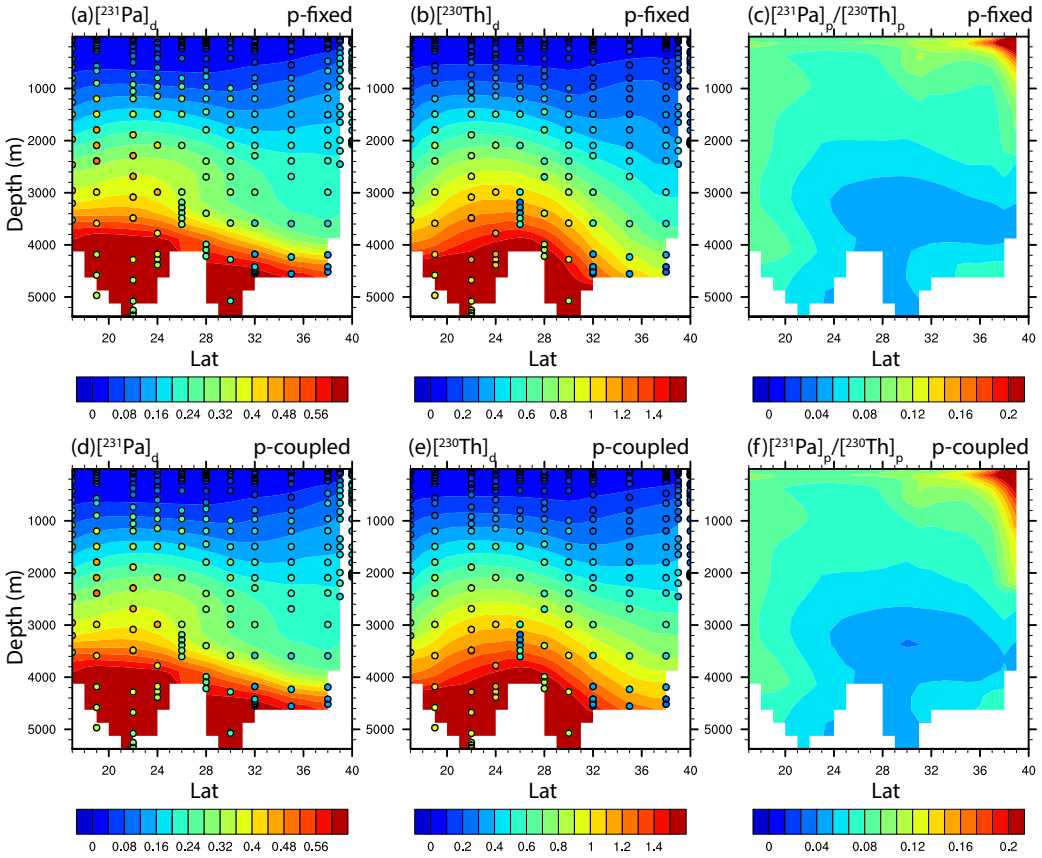

Figure 3. Dissolved ^{231}Pa, dissolved ^{230}Th and particulate ^{231}Pa/^{230}Th in CTRL along GEOTRACES transect GA03 (Hayes et al., 2015) (the track is indicated in Fig. S4) for both p-fixed and p-coupled ^{231}Pa and ^{230}Th. Observations of dissolved ^{231}Pa and ^{230}Th activity are superimposed using the same colormap.

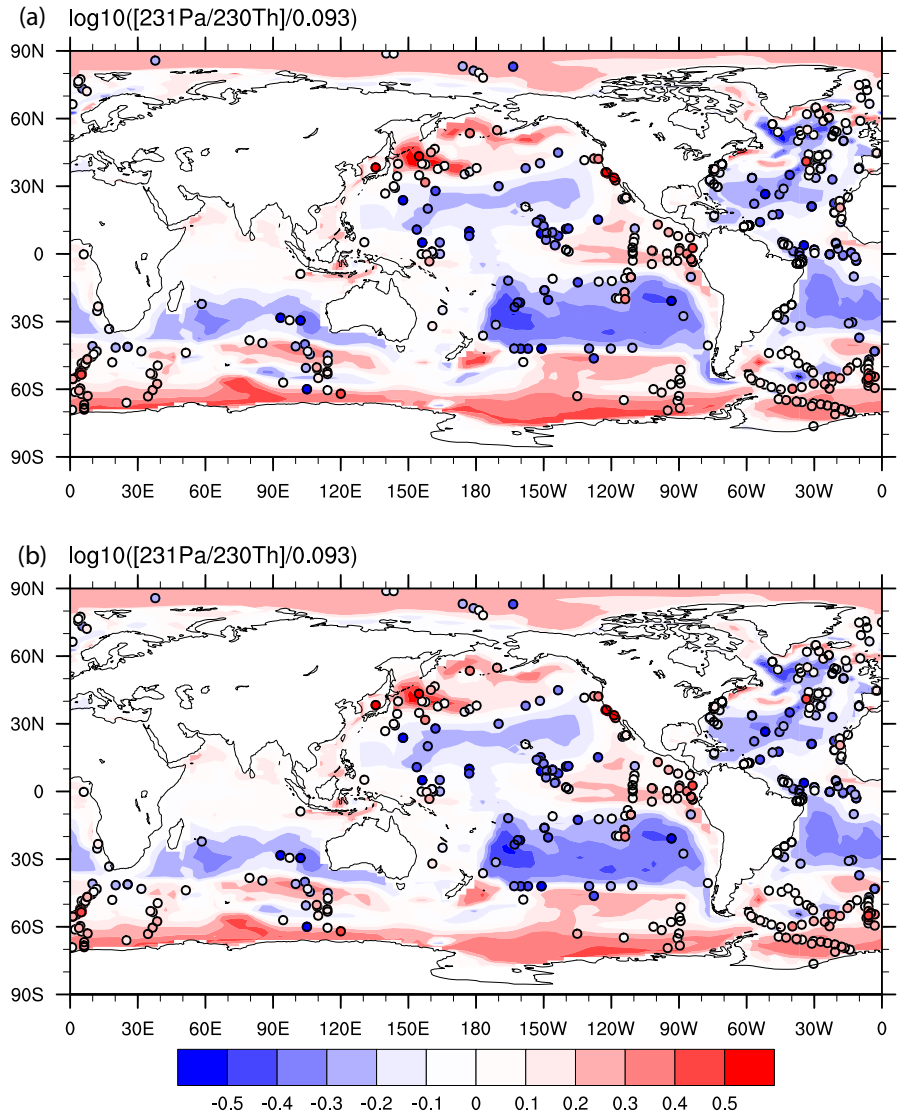

Figure 4. Sediment $^{231}Pa/^{230}Th$ activity ratio in CTRL for both p-fixed (a) and p-coupled version (b). Observations are attached as filled cycles using the same color map. The $^{231}Pa/^{230}Th$ activity ratio is plotted relative to the production ratio of 0.093 on a $\log_{10}$ scale.

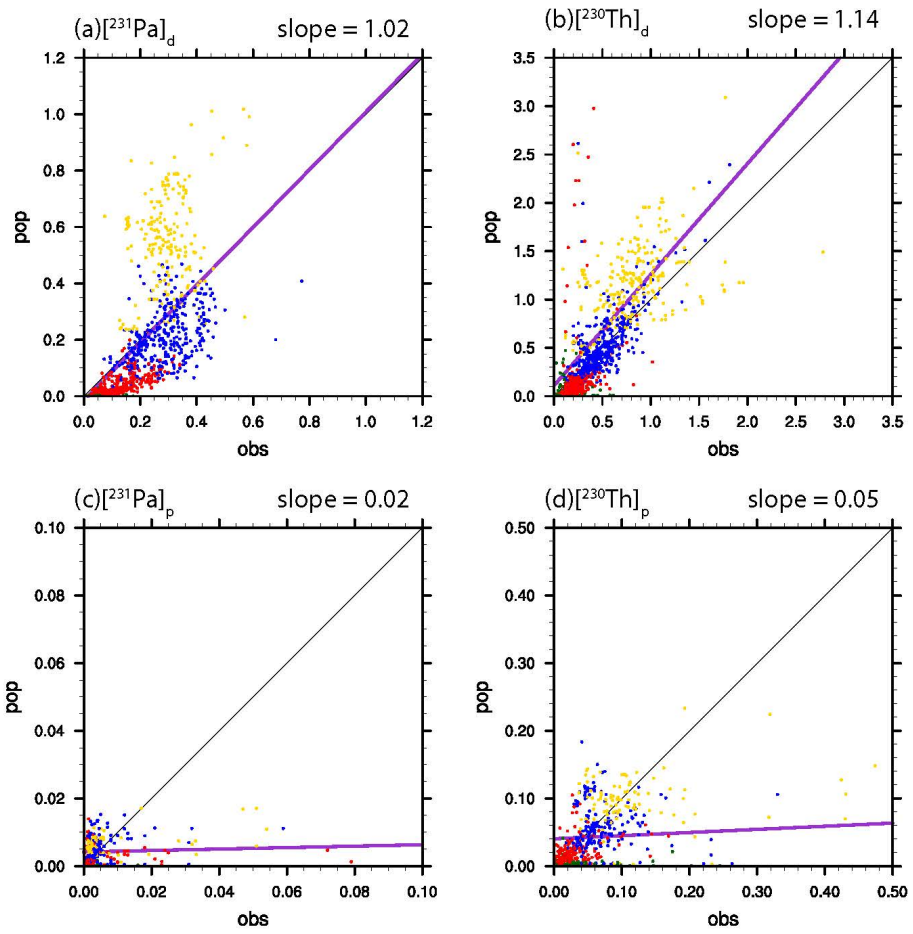

Figure 5. Scatter plot of global dissolved and particulate ^{231}Pa and ^{230}Th between observation and CTRL (p-fixed) (unit: dpm/m^3). (a) dissolved ^{231}Pa; (b) particulate ^{231}Pa; (c) dissolved ^{230}Th; (d) particulate ^{230}Th. Observations in different depth range are indicated by different colors: green for 0-100m; red for 100m-1000m; blue for 1000m-3000m and yellow for deeper than 3000m. Purple line is the least squared linear regression line and slope is the linear regression coefficient.

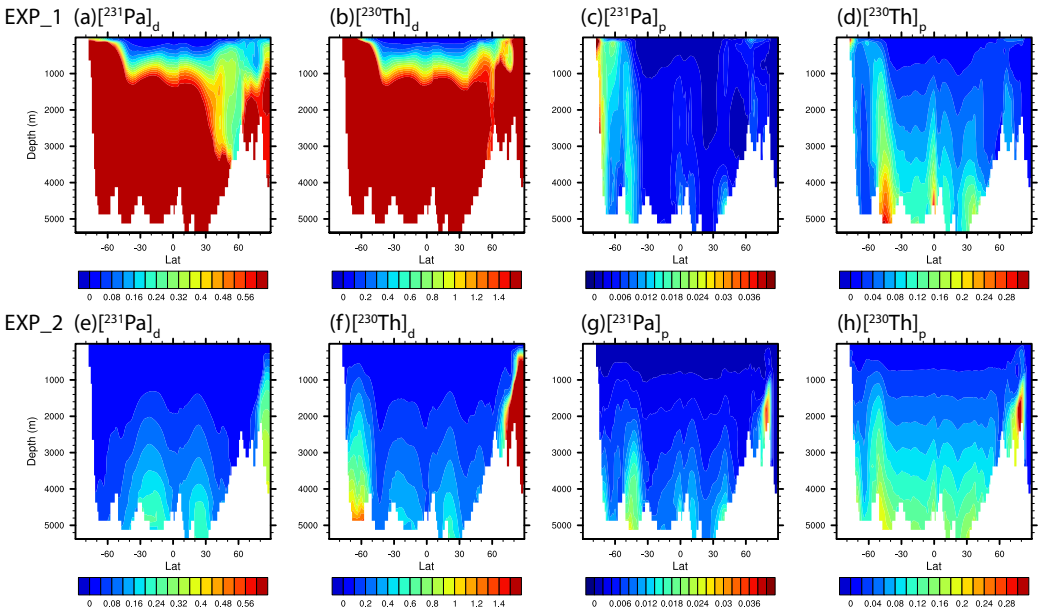

Figure 6. Atlantic zonal mean dissolved and particulate ^{231}Pa and ^{230}Th in EXP_1 and EXP_2 (unit: dpm/m^3). EXP_1: (a) dissolved ^{231}Pa; (b) dissolved ^{230}Th; (c) particulate ^{231}Pa; (d) particulate ^{230}Th. EXP_2: (e) dissolved ^{231}Pa; (f) dissolved ^{230}Th; (g) particulate ^{231}Pa; (h) particulate ^{230}Th.

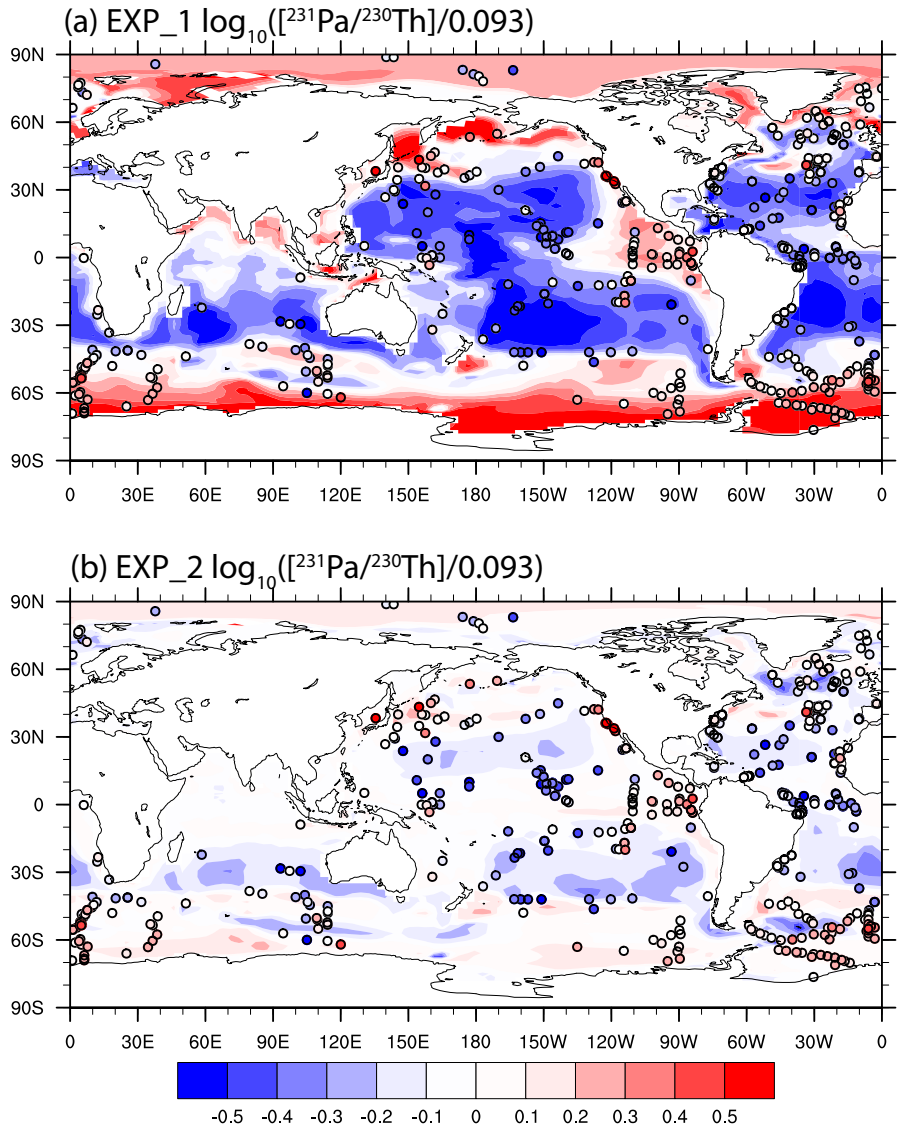

923

924 Figure 7. Sediment $^{231}Pa/^{230}Th$ activity ratio in EXP_1 (a) and EXP_2 (b).
925 Observations are attached as filled cycles using the same color map. The $^{231}Pa/^{230}Th$
926 activity ratio is plotted relative to the production ratio of 0.093 on a $\log_{10}$ scale.

927

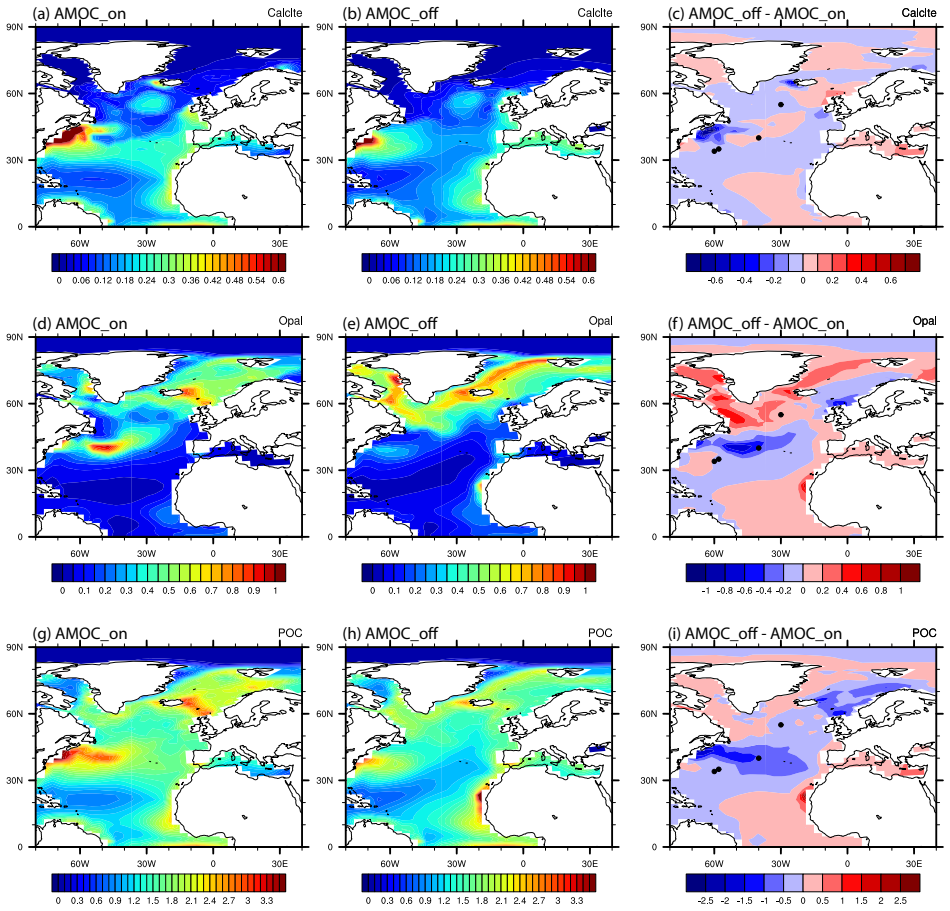

928

929 Figure 8. Comparison of particle fluxes between AMOC_on and AMOC_off. $CaCO_3$ flux
930 at 105m (mol m^{-2} yr^{-1}) during AMOC_on (a), AMOC_off (b) and difference between
931 AMOC_off and AMOC_on. (b) Opal flux at 105m (mol m^{-2} yr^{-1}) during AMOC_on (d),
932 AMOC_off (e) and difference between AMOC_off and AMOC_on (f). POC flux at 105m
933 (mol m^{-2} yr^{-1}) during AMOC_on (g), AMOC_off (h) and difference between AMOC_off
934 and AMOC_on (i).

935

936

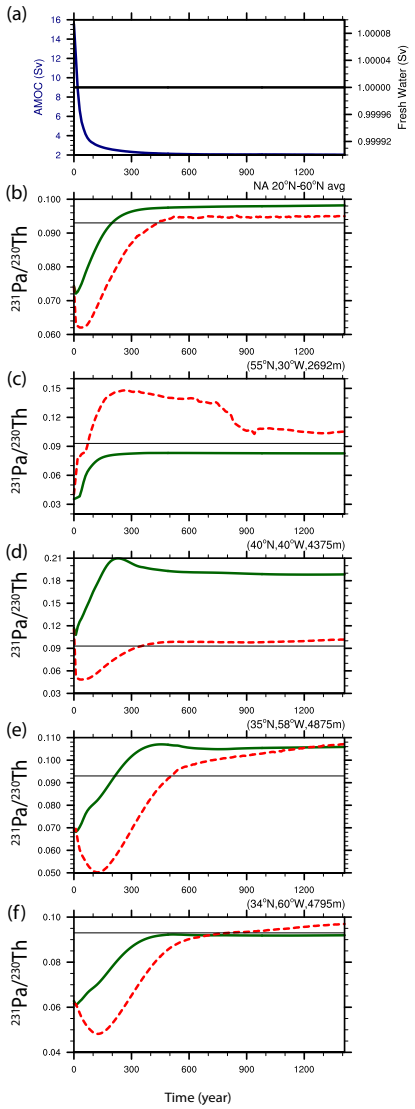

Figure 9. Time evolutions in HOSING. (a) Freshwater forcing (black) and AMOC strength (navy), which is defined as the maximum of the overturning streamfunction below 500m in the North Atlantic. (b) North Atlantic average sediment $^{231}Pa/^{230}Th$ activity ratio from 20°N to 60°N: p-fixed (green) and p-coupled (red). Production ratio of 0.093 is indicated by a solid black line (similar in c, d, e and f). (c) Sediment $^{231}Pa/^{230}Th$ activity ratio at (55°N, 30°W). (d) Sediment $^{231}Pa/^{230}Th$ activity ratio at (40°N, 40°W). (e) Sediment $^{231}Pa/^{230}Th$ activity ratio at (35°N, 58°W). (f) Sediment $^{231}Pa/^{230}Th$ activity ratio at (34°N, 60°W). (e) and (f) are near Bermuda Rise. Locations of each site are shown as dots in Fig. 8b.

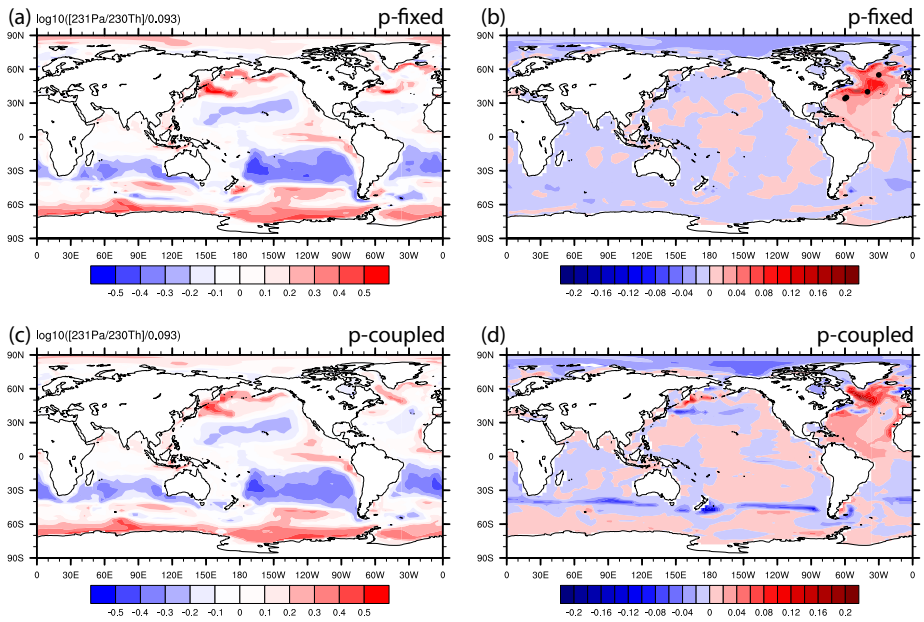

Figure 10. Sediment $^{231}Pa/^{230}Th$ activity ratio during AMOC off state and the difference between AMOC off and CTRL. (a) P-fixed $\log_{10}([^{231}Pa/^{230}Th]/0.093)$ in AMOC_off. (b) Difference of p-fixed sediment $^{231}Pa/^{230}Th$ activity ratio between AMOC_off and AMOC_on. (c) and (d) are similar to (a) and (b) for p-coupled sediment $^{231}Pa/^{230}Th$ activity ratio. Black dots in (b) shows the locations of sites in Fig. 7 from North to South.

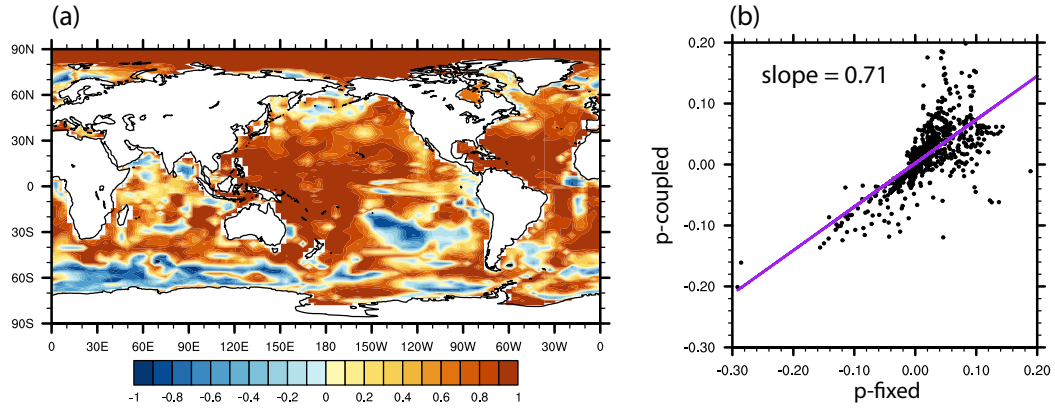

Figure 11. (a) Correlation of p-fixed and p-coupled evolution of sediment $^{231}Pa/^{230}Th$ activity ratio in HOSING. (b) Scatter plot of p-fixed and p-coupled sediment $^{231}Pa/^{230}Th$ activity ratio change from AMOC_on to AMOC_off in the Atlantic and the Southern Ocean (70°W-20°E). Purple line is the least squared linear regression line and slope is the linear regression coefficient.

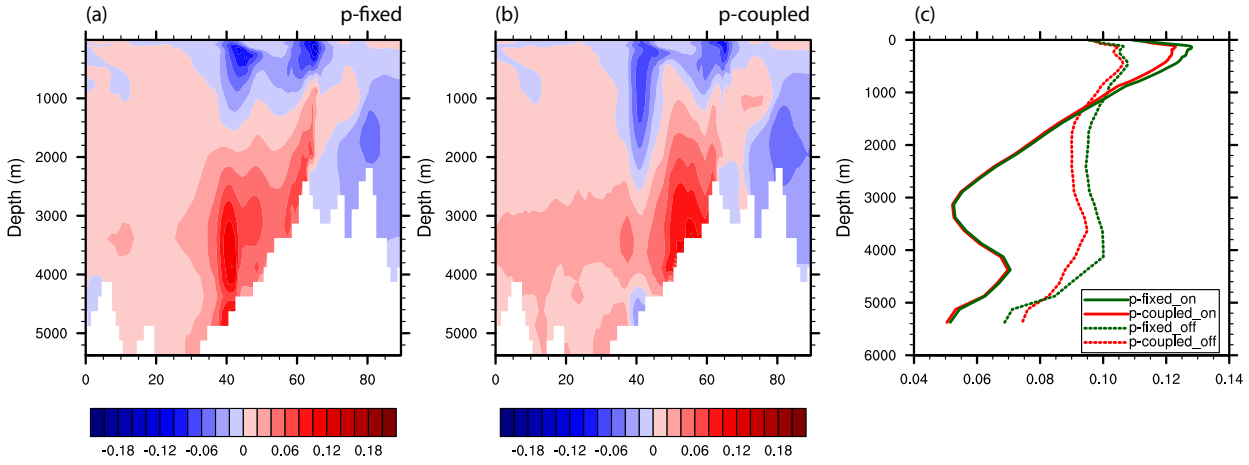

Figure 12. Difference of Atlantic zonal mean particulate $^{231}Pa/^{230}Th$ between AMOC_off and AMOC_on: (a) p-fixed and (b) p-coupled. (c) North Atlantic (20°N-60°N) average profile during AMOC_on (solid) and AMOC_off (dash) for p-fixed (green) and p-coupled (red) particulate $^{231}Pa/^{230}Th$.

970

971

972

973